ORIGINAL RESEARCH

RNA Sequencing Reveals the Activation of Wnt Signaling in Low Flow Rate Brain Arteriovenous Malformations

Ran Huo, MD;* Weilun Fu, MD;* Hao Li, MD; Yuming Jiao, MD; Zihan Yan, MD; Linjian Wang, MS; Jie Wang, MD; Shuo Wang, MD; Yong Cao, MD; Jizong Zhao, MD

***Background*—**The blood flow rate of brain arteriovenous malformations (bAVMs) is an important clinical characteristic closely associated with the hemorrhage risk and radiosurgery obliteration rate of bAVMs. However, the underlying molecular properties remain unclear. To identify potential key molecules, signaling pathways, and vascular cell types involved, we compared gene expression profiles between bAVMs with high flow rates and low flow rates (LFR) and validated the functions of selected key molecules in vitro.

***Methods and Results*—**We performed RNA-sequencing analysis on 51 samples, including 14 high flow rate bAVMs and 37 LFR bAVMs. Functional pathway analysis was performed to identify potential signals influencing the flow rate phenotype of bAVMs. Candidate genes were investigated in bAVM specimens by immunohistochemical staining. Migration, tube formation, and proliferation assays were used to test the effects of candidate genes on the phenotypic properties of cultured human umbilical vein endothelial cells and human brain vascular smooth muscle cells. We identified 250 upregulated and 118 downregulated genes in LFR bAVMs compared with high flow rate bAVMs. Wnt signaling was activated in the LFR group via upregulation of FZD10 and MYOC. Immunohistochemical staining showed that vascular endothelial and smooth muscle cells of LFR bAVMs exhibited increased FZD10 and MYOC expression. Experimentally elevating these genes promoted human umbilical vein endothelial cells and migration and tube formation by activating canonical Wnt signaling in vitro.

***Conclusions*—**Our results suggest that canonical Wnt signaling mediated by FZD10 and MYOC is activated in vascular endothelial and smooth muscle cells in LFR bAVMs. **(*J Am Heart Assoc*. 2019;8:e012746. DOI: 10.1161/JAHA.119.012746.)**

Key Words: intracranial arteriovenous malformations • gene expression • hemodynamics • Wnt signaling pathway

Brain arteriovenous malformations (bAVMs) consist of abnormal tangles of dilated vascular structures, called a nidus, which connect arteries and veins directly without the intervening capillary beds.[1] They are one of the major causes of intracranial hemorrhage and/or subarachnoid hemorrhage, leading to substantial morbidity and mortality, especially in children and young adults.[2,3] Current intervention options include neurosurgery, embolization, and stereotactic radiotherapy. The primary goal of these interventions is to prevent new or recurrent hemorrhage, but all these procedures have considerable risks and complications.[4,5]

The blood flow rate is regarded as an important clinical characteristic that is closely associated with hemorrhage risk, obliteration rate after radiosurgery, and the occurrence of normal perfusion pressure breakthrough after surgical resection.[6–8] Generally, the blood flow rate reflects the hemodynamic and angioarchitectural features of bAVMs, including an imbalance between inflow and outflow, vascular resistance, and morphological patterns.[9,10] Although the blood flow rate of bAVMs is important, the underlying molecular mechanisms remain unclear.

Studies investigating differences in gene expression in bAVMs with different flow rates may identify genes and pathways involved in this phenotype. Previous studies on bAVM transcriptomes were small scale and used microarray

From the Department of Neurosurgery, Beijing Tiantan Hospital, Capital Medical University, Beijing, China (R.H., W.F., H.L., Y.J., Z.Y., J.W., S.W., Y.C., J.Z.); China National Clinical Research Center for Neurological Diseases, Beijing, China (R.H., W.F., H.L., Y.J., Z.Y., J.W., S.W., Y.C., J.Z.); Center of Stroke, Beijing Institute for Brain Disorders, Beijing, China (R.H., W.F., H.L., Y.J., Z.Y., J.W., S.W., Y.C., J.Z.); Beijing Key Laboratory of Translational Medicine for Cerebrovascular Disease, Beijing, China (R.H., W.F., H.L., Y.J., Z.Y., J.W., S.W., Y.C., J.Z.); Savaid Medical School, University of the Chinese Academy of Sciences, Beijing, China (L.W., J.Z.).

Accompanying Data S1, Tables S1 through S3 and Figure S1 are available at https://www.ahajournals.org/doi/suppl/10.1161/JAHA.119.012746

*Dr Huo and Dr Fu contributed equally to this work.

Correspondence to: Yong Cao, MD, Department of Neurosurgery, Beijing Tiantan Hospital, Capital Medical University, 119 South Fourth Ring Rd West, Fengtai District, Beijing, 100071, China. E-mail: caoyong@bjtth.org

Received March 21, 2019; accepted May 17, 2019.

Clinical Perspective

What Is New?

- RNA-sequencing of brain arteriovenous malformation (bAVM) tissue revealed differences in gene expression profiles of bAVMs with different blood flow rate phenotypes.
- FZD10 and MYOC were upregulated and Wnt signaling was activated in the low flow rate bAVMs.
- We found that overexpression of FZD10 and MYOC could activate canonical Wnt signaling and promote angiogenesis responses in endothelial and smooth muscle cells, which might induce high resistance and lead to low blood flow rate phenotypes.

What Are the Clinical Implications?

- The blood flow rate of bAVMs is closely associated with the hemorrhage risk, obliteration rate after radiosurgery, and occurrence of normal perfusion pressure breakthrough after surgical resection.
- The current study may help identify the potential causes of different blood flow phenotypes and provide a possibility for medical treatment to prevent bAVM rupture.

techniques.[11,12] RNA-sequencing (RNA-Seq) is a more advanced gene expression analysis method that can identify biomarkers across the broadest range of mRNAs with high efficiency and sensitivity.[13] In our study, we divided bAVM patients into a high flow rate (HFR) group and a low flow rate (LFR) group according to the blood flow rate obtained from radiological information. RNA-Seq was performed on the bAVM surgical samples, and we investigated the differentially expressed genes and related pathways between the 2 groups. The functions of differentially expressed genes of interest were further investigated in vitro. Our findings may help identify the mechanisms behind the different blood flow phenotypes and provide a possibility for medical treatment to prevent progression or bleeding of bAVMs.

Methods

The data that support the findings of this study are available from the corresponding author upon reasonable request.

Patients and Samples

All study participants were Chinese and recruited at Beijing Tiantan Hospital, Capital Medical University. Samples were collected from consecutive patients who underwent surgical treatment for bAVMs in our department. Hereditary hemorrhagic telangiectasia was clinically excluded according to the Curaçao Criteria.[14] Patients whose samples passed quality control for RNA-Seq were enrolled in our study. Finally, 51 patients were enrolled from September 2016 to November 2017. All subjects provided informed consent, and the study was approved by the institutional review board of Beijing Tiantan Hospital, Capital Medical University. Clinical diagnoses were confirmed by digital subtraction angiography and histologic evaluation in the hospital's pathology department. For sample preparation, once the bAVM was resected, the brain tissue was removed in the operating room, and 2 to 3 g bAVM tissue was collected for RNA-Seq. Specimens were stored in liquid nitrogen within 5 minutes.

Radiological Review

All patients underwent simultaneous biplanar digital subtraction angiography as the diagnostic method or part of a treatment plan with an image frame rate of 4 frames per second and injector-controlled contrast injection rates (4 cm^3/s for a total of 8 cm^3). Angiographic, magnetic resonance, and computed tomography images available for each patient were evaluated by consensus between 2 researchers who were blinded to the clinical information. The blood flow rate of AVMs was estimated as previously described by determining the number of digital subtraction angiography frames between the first depiction of the nidus and the first visualization of a vein (HFR: venous drainage seen in <2 frames after nidal visualization; LFR: venous drainage seen in 2 or more frames after nidal visualization).[9]

RNA Isolation, Library Preparation, and Sequencing

Total RNA was isolated using the TRIzol method. Then, RNA degradation and contamination were monitored on 1% agarose gels. We checked RNA purity by using a NanoPhotometer spectrophotometer (IMPLEN, CA), and RNA concentration was measured using a Qubit RNA Assay Kit with a Qubit 2.0 Fluorometer (Life Technologies, CA). RNA integrity was assessed using an RNA Nano 6000 Assay Kit with a Bioanalyzer 2100 system (Agilent Technologies, CA).

A total amount of 4 μg RNA per sample was used as input material for the RNA sample preparations. Ribosomal RNA was removed by using an Epicentre Ribo-zero rRNA Removal Kit (Epicentre, WI), and the rRNA-free residue was cleaned by ethanol precipitation. Sequencing libraries were generated using rRNA-depleted RNA with an NEBNext Ultra Directional RNA Library Prep Kit for Illumina (NEB, MA) following the manufacturer's recommendations. Fragmentation was carried out using divalent cations at an elevated temperature in NEBNext First Strand Synthesis Reaction Buffer (5X). First strand cDNA was synthesized using a random hexamer primer and M-MuLV Reverse Transcriptase (RNaseH-). Second strand cDNA synthesis

was subsequently performed using DNA Polymerase I and RNase H. In the reaction buffer, dTTP was replaced by dUTP. The remaining overhangs were converted into blunt ends via exonuclease/polymerase activities. After adenylation, the 3′ ends of DNA fragments were ligated with NEBNext Adaptors with a hairpin loop structure to prepare for hybridization. The library fragments were purified with an AMPure XP system (Beckman Coulter, Beverly, MA). Then, 3 μL USER Enzyme (NEB, MA) was used with cDNA at 37°C for 15 minutes followed by 5 minutes at 95°C before polymerase chain reaction. Polymerase chain reaction was then performed with Phusion High-Fidelity DNA polymerase, Universal polymerase chain reaction primers, and Index (X) Primer. Finally, the products were purified (AMPure XP system), and the library quality was assessed on an Agilent Bioanalyzer 2100. The clustering of the index-coded samples was performed on a cBot Cluster Generation System using a TruSeq PE Cluster Kit v3-cBot-HS (Illumina) according to the manufacturer's instructions. After cluster generation, the libraries were sequenced on the Illumina HiSeq platform, and 150-bp paired-end reads were generated.

Quality Control and Data Analysis

Raw data in fastq format were first processed through in-house Perl scripts. In this step, clean data were obtained by removing reads containing adaptors, reads containing poly-N, and low-quality reads from the raw data. At the same time, Q20, Q30, and GC content of the clean data were calculated. All downstream analyses were based on high-quality clean data. Reference genome and gene model annotation files were downloaded directly from the genome website. The index of the reference genome was built using bowtie2 v2.2.8, and paired-end clean reads were aligned to the reference genome using Hisat2 v2.0.5.

Hg19 RefSeq (RNA sequences, GRCh37) was downloaded from the UCSC Genome Browser (http://genome.ucsc.edu). The clean reads were aligned with both genome hg19 and transcript reference using STAR v2.2.1, and gene expression was calculated by RSEM v1.3.0 using FPKM (fragments per kilobase of exon per million fragments mapped). Transcripts with a $P<0.05$ were considered differentially expressed. Functional enrichment analysis of upregulated genes (fold change ≥ 2, $P<0.01$) in LFR bAVMs was implemented by the WebGestalt website (http://webgestalt.org/option.php), including Gene Ontology and Kyoto Encyclopedia of Genes and Genomes. Terms with P values <0.05 were considered significantly enriched in differentially expressed genes. R v3.5.1 was used for analysis of the gene expression data.

Immunohistochemistry

The tissue sections were incubated with primary antibody, FZD10 (1:500, ab150564, Abcam) or MYOC (1:500, ab41552, Abcam), overnight at 4°C and then incubated with a biotinylated secondary antibody at room temperature for 1 hour, followed by incubation with horseradish peroxidase-labeled streptavidin for 30 minutes. After washing with Tris-buffer, the sections were stained with diamino benzidine, and nuclei were counterstained with hematoxylin. Specimens were observed, and images were captured with an EVOS FL Auto 2 Imaging System (Invitrogen). We measured the expression semiquantitatively as previously described.[15] Scoring of immunoreactivity was as follows: 0, no staining; 1, mild staining; 2, moderate staining; and 3, intense staining. Two researchers who were blinded to the clinical information performed the measurements, and data were collected as the average of the 2 observations.

Cell Culture and Treatment

Human umbilical vein endothelial cells (HUVECs) were isolated from umbilical veins (ScienCell, Carlsbad, CA). Cells were cultured in endothelial cell medium (ScienCell) supplemented with endothelial cell growth supplement and 5% fetal bovine serum (ScienCell). Human brain vascular smooth muscle cells (HBVSMCs) were isolated from arteries and arterioles of the human brain (ScienCell) and were cultured in smooth muscle cell basal medium (ScienCell) supplemented with smooth muscle cell growth supplement and 2.5% fetal bovine serum (ScienCell). All cells were cultured according to the recommended protocols. For plasmid DNA transfection, cells were transfected with a GV219 vector expressing FZD10 or MYOC using Lipofectamine 3000 (Invitrogen) according to the manufacturer's instructions. As controls, cells were transfected in parallel with a GV219 empty vector without the insert.

Reverse Transcription Quantitative Polymerase Chain Reaction

Total RNA was isolated from transfected cells using the TRIzol reagent (Invitrogen). RNA was cleaned with gDNA Eraser (Takara) to remove DNA contamination. One microgram of purified RNA was reverse transcribed using a PrimeScript RT reagent Kit (Takara). Quantitative polymerase chain reaction was performed using TB Green Premix Ex Taq (Takara) with a QuantStudio 3 System (Applied Biosystems) with specific primers designed for amplicons of 75 to 150 bp. GAPDH was used as a reference gene. The primer sequences are listed in Table S1.

Statistical Analysis

Statistical analyses were accomplished by using PRISM (GraphPad version 7.0) and SPSS (version 25.0). For clinical data, patients with HFR or LFR bAVMs were compared using descriptive

statistics. For age and Spetzler-Martin grade, Mann–Whitney *U* tests were performed. Sex and hemorrhage were compared using Pearson χ^2 tests. Fisher exact tests were used to compare seizure, deep venous drainage, perforating artery, and location. The Mann–Whitney *U* tests were used to investigate the differential expression of FZD10 and MYOC in tissue sections, and Student *t* tests were used to analyze the results of in vitro experiments. All results are expressed as the mean±SD. $P<0.05$ was considered to indicate statistical significance in all cases.

Additional methodologies are described in Data S1.

Results

bAVM Flow Rate Types and Other Characteristics of the Study Population

A total of 51 patients with bAVMs were included in our study. None of the patients had familial bAVM or hereditary hemorrhagic telangiectasia. The bAVMs were further classified as HFR (n=14, 27.45%) or LFR (n=37, 72.55%) according to the flow types indicated by digital subtraction angiography (Figure 1). No significant differences were found between the 2 groups regarding sex, history of seizure, hemorrhagic presentation, or angioarchitectural features. The baseline characteristics of all patients are summarized in Table.

Differential Expression Profile Between HFR and LFR bAVMs

The analysis compared gene expression profiles between 14 HFR bAVMs and 37 LFR bAVMs to identify genes showing consistent differences in expression. A total of 368 genes were identified as differentially expressed (Figure 2A), and 250 genes presented more than 2-fold upregulated expression in LFR bAVMs (Table S2). A marked upregulation of SBK3 expression was seen in LFR bAVMs with a 9.5-fold change. In

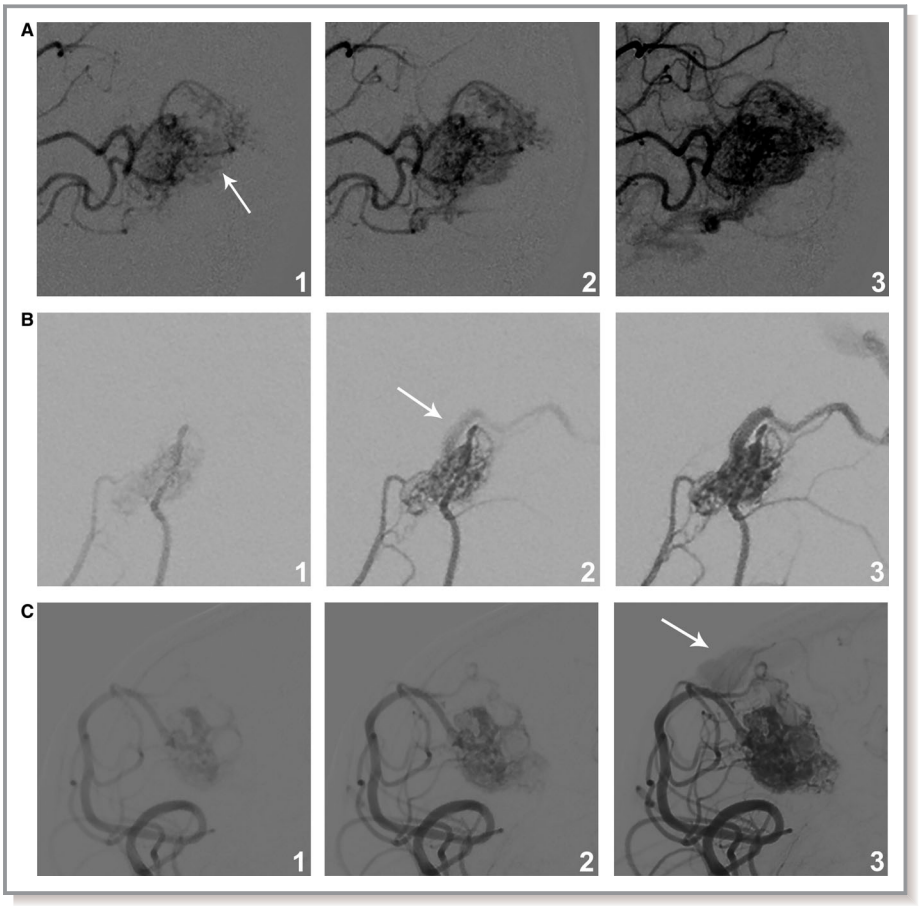

Figure 1. bAVM blood flow rate subtypes. The blood flow rate was classified as high if the vein was visible at the same time as the nidus (**A**) or at 1 frame after visualization of the nidus (**B**), and the blood flow rate was classified as low if the vein was visualized later than 2 frames after depiction of the nidus (**C**). The same frame rate of 4 images per second was used in all instances, and machine-assisted injections with a constant rate increase were performed. The arrows denote the first visualization of the vein. bAVM indicates brain arteriovenous malformations.

addition, the expression of 118 genes was downregulated by more than 2-fold in LFR bAVMs (Table S2), and the most obvious decrease in expression of LFR bAVMs was observed for IGHV3-9, with an 8.3-fold change.

Wnt Signaling Is Activated in LFR bAVMs

To identify potential functional pathways that influence the flow rate phenotype of bAVMs, we performed Gene Ontology and Kyoto Encyclopedia of Genes and Genomes analysis of differentially expressed genes. Gene Ontology analysis identified that Wnt signaling, an important signaling pathway associated with embryonic angiogenesis and the development of bAVMs,[15,16] was activated in the LFR group with the upregulation of FZD10 and MYOC (Figure 2B; Table S3). FZD10 is a member of the family of Frizzled proteins, which are 7-transmembrane domain proteins, and is known as a receptor of WNT7b, which may influence downstream molecules through Wnt signaling.[17,18] MYOC belongs to a family of glycosylated proteins containing a C-terminal olfactomedin domain and can interact with secreted inhibitors of Wnt signaling, such as sFRP1 and sFRP3, as a modulator of the Wnt signaling pathway.[19,20]

FZD10 and MYOC were found in the noncanonical Wnt signaling pathway via Jun N-terminal kinase and MAPK in Gene Ontology analysis, and Kyoto Encyclopedia of Genes and Genomes pathway analysis did not identify which type of Wnt signaling, canonical or noncanonical, was affected by the 2 molecules (Figure 2B; Table S3). Further investigation of differentially expressed genes (including a fold change <2) found that AXIN2 and TCF7L2, the target genes of the canonical Wnt pathway, showed 1.2- ($P<0.05$) and 1.3-fold ($P<0.05$) increases in expression in the LFR group, respectively. The expression of FZD10, MYOC, and downstream molecules of the canonical Wnt signaling pathway in bAVMs with different blood flow rates are shown in Figure 2C. The specific functions of FZD10 and MYOC in canonical or noncanonical Wnt signaling need to be verified in vascular cells.

FZD10 and MYOC Are Relatively Highly Expressed in Vascular Endothelial Cells and Smooth Muscle Cells of LFR bAVMs

To validate the differential expression of FZD10 and MYOC at the protein level and investigate the cell types expressing them, we performed immunohistochemistry on bAVM specimens. We detected the expression of FZD10 and MYOC in 44 specimens (LFR, n=37; HFR, n=14). Immunohistochemistry analysis revealed the expression of FZD10 in 26 samples (23/30 LFR and 3/14 HFR) and MYOC in 38 samples (30/30 LFR and 8/14 HFR). FZD10 was observed in vascular endothelial cells (ECs), smooth muscle cells (SMCs) (Figure 3A), and brain tissues far from the nidus. MYOC was also detected in ECs and SMCs of bAVMs (Figure 3B). We observed that the expression levels of FZD10 and MYOC in ECs and SMCs showed the same trend.

Semiquantitative grading of FZD10 and MYOC expression levels was performed in the vascular structures of bAVMs (Figure 3C). FZD10 had a relatively low expression level of 0.21 ± 0.11 in HFR bAVMs, while the expression level reached 1.37 ± 0.18 in LFR bAVMs ($P<0.001$). The expression level of MYOC was 1.07 ± 0.32 in HFR bAVMs and 2.60 ± 0.10 in LFR bAVMs ($P<0.001$). The results were consistent with RNA-Seq analysis.

FZD10 and MYOC Improve Cell Migration and Tube Formation of HUVECs and HBVSMCs

To investigate the functional significance of FZD10 and MYOC in the ECs and SMCs of bAVMs, we transfected HUVECs and HBVSMCs with FZD10- or MYOC-overexpressing plasmids and GV219 empty vector. The results of reverse transcription polymerase chain reaction suggested that HUVECs and HBVSMCs expressed low levels of FZD10

Table. Baseline Characteristics of the Study Participants

Characteristic	High Flow Rate (n=14)	Low Flow Rate (n=37)	*P* Value
Sex, female	3 (21%)	18 (49%)	0.078
Age, y	33±19	27±14	0.347
Clinical presentation			
Seizure	4 (29%)	14 (38%)	0.744
Hemorrhage	7 (50%)	18 (49%)	0.931
Angioarchitectural features			
Deep venous drainage	1 (7%)	13 (35%)	0.077
Perforating artery	0 (0%)	4 (11%)	0.565
Location			
Frontal	6 (43%)	15 (41%)	0.835
Temporal	4 (29%)	10 (27%)	
Parietal	2 (14%)	8 (22%)	
Occipital	2 (14%)	2 (5%)	
Cerebellar	0 (0%)	2 (5%)	
Spetzler-Martin			
1	5 (36%)	5 (14%)	0.030*
2	6 (43%)	12 (32%)	
3	2 (14%)	14 (38%)	
4	1 (7%)	6 (16%)	
5	0 (0%)	0 (0%)	

*P value indicates statistical significance ($P\leq0.05$).

and MYOC mRNA (Figure S1); therefore, we did not try to downregulate their expression by siRNA. We determined optimal transfection concentrations and confirmed that the plasmids were taken up by cells and expressed (Figure 4A). Several assays were performed to test the effects of FZD10 or MYOC upregulation on tube formation, cell migration, and cell proliferation. After transfection with FZD10-over-expressing plasmids, increased mobility of transfected cells was observed in wound healing assays (Figure 4B), and the microvasculature formed by HUVECs and HBVSMCs was significantly increased compared with that of the control cells (Figure 4C). Similar findings were also apparent in tube formation and wound healing assays of MYOC-transfected HUVECs and HBVSMCs (Figure 4B and 4C). However, FZD10 or MYOC did not influence the proliferation of HUVECs and HBVSMCs (data not shown). These results suggest that FZD10 and MYOC can promote the angiogenesis responses of HUVECs and HBVSMCs by changing the biological behavior of cells.

FZD10 and MYOC Activate Canonical β-Catenin/Wnt Signaling in HUVECs and HBVSMCs

Previous studies found that FZD10 and MYOC could activate both canonical and noncanonical Wnt signaling.[18,20–22] To investigate the specific pathway modulated by the 2 genes,

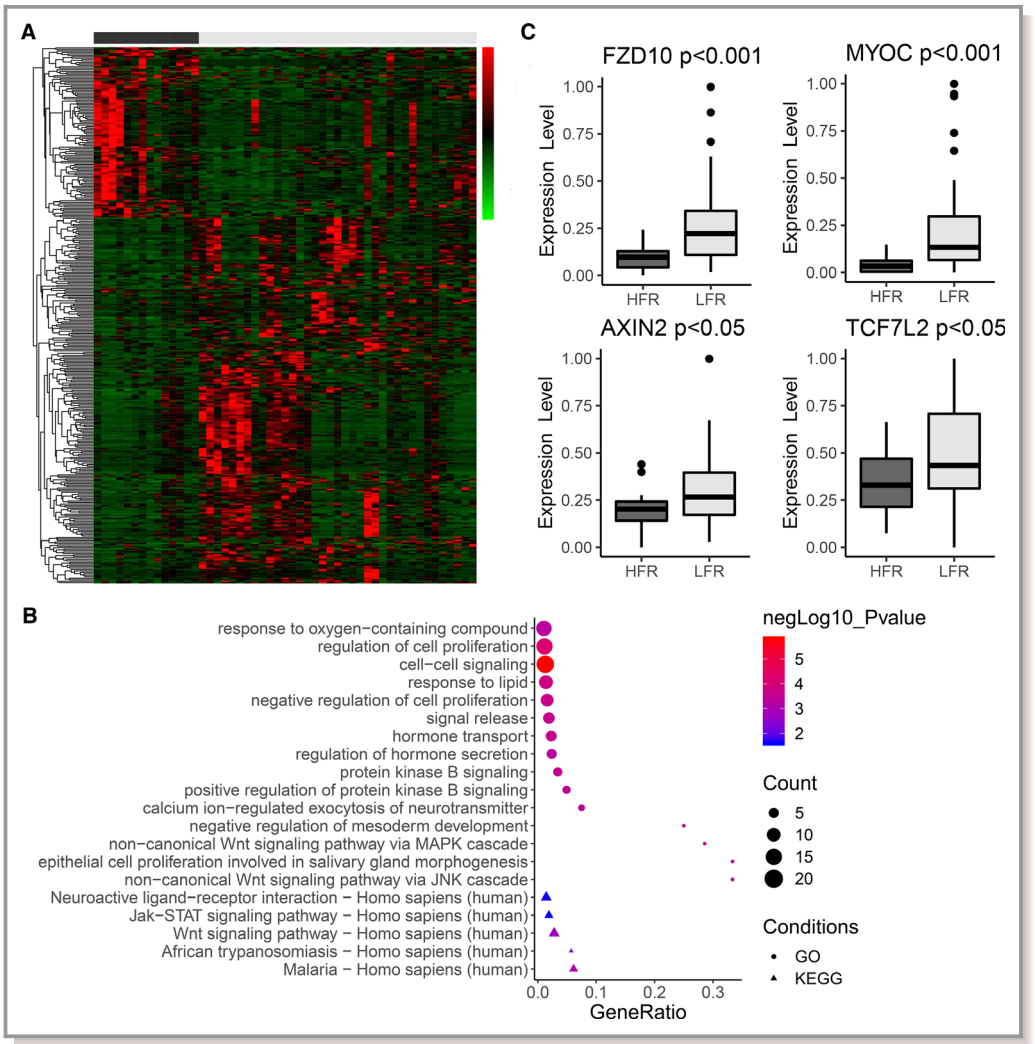

Figure 2. mRNA expression profiling in bAVMs. **A**, Gene expression heatmap of differentially expressed mRNAs ($P \leq 0.05$ and fold change ≥ 2 or ≤ 0.5) in HFR vs LFR bAVM tissues. The *x*-axis shows each bAVM patient (black=HFR; gray=LFR), and the *y*-axis shows individual genes. In the heatmap cells, red indicates high gene expression (ie, upregulated expression) relative to the median expression; green indicates low expression (ie, downregulated expression); black indicates that expression is similar to the median. **B**, Top 15 terms of GO analysis (ranked by *P* value) and KEGG analysis enriched by upregulated genes in LFR bAVMs. **C**, The expression levels of FZD10, MYOC, and downstream molecules in canonical Wnt signaling. bAVM indicates brain arteriovenous malformations; HFR, high flow rate; LFR, low flow rate.

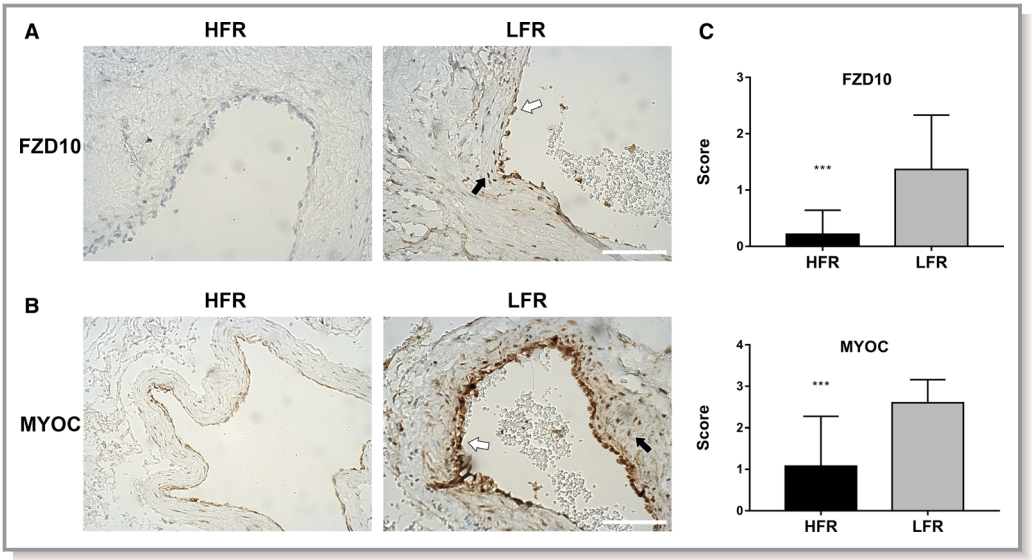

Figure 3. Detection of FZD10 and MYOC in bAVM tissue samples. Immunohistochemical staining of bAVM tissue samples with differential flow rate subtypes show strong staining for FZD10 (**A**) and MYOC (**B**) in LFR bAVM tissue. Endothelial cells lining the vascular lumen (white arrows) and vascular smooth muscle cells in the vessel wall (black arrows) both show staining for FZD10 and MYOC. The scale bar corresponds to 200 μm. **C**, Semiquantitative grading of FZD10 and MYOC expression levels in the vascular structure of bAVMs. ***P<0.001. bAVM indicates brain arteriovenous malformations; HFR, high flow rate; LFR, low flow rate.

we detected the downstream molecules of canonical and noncanonical Wnt signaling in HUVECs and HBVSMCs. Overexpression of FZD10 in HUVECs and HBVSMCs increased the mRNA levels of AXIN2 and TCF-1 (Figure 5D), the target genes of the canonical Wnt pathway. In contrast, FZD10 did not influence Jun N-terminal kinase activation (Figure 5E), a hallmark of noncanonical Wnt activation. After transfection with FZD10, the total level of β-catenin in HUVECs was elevated slightly, which might mean that the degradation of β-catenin was inhibited (Figure 5E). However, the total level of β-catenin in HBVSMCs remained unchanged. Although β-catenin did not show an obvious increase, its nuclear translocation in both HUVECs and HBVSMCs was confirmed by immunofluorescence (Figure 5A, 5B, and 5C), which is direct evidence of canonical Wnt pathway activation.

Similarly, transfection of HUVECs and HBVSMCs with the MYOC-overexpressing plasmid led to the upregulation of AXIN2 and TCF-1 and did not influence the phosphorylation of Jun N-terminal kinase (Figure 5D and 5E). In agreement with canonical Wnt pathway activation, nuclear β-catenin staining was also enhanced in HUVECs and HBVSMCs (Figure 5A, 5B, and 5C), even if the total level of β-catenin did not change noticeably.

Discussion

The blood flow rate of bAVMs is an important hemodynamic parameter that can influence the clinical decision and efficacy of treatments.[7,9] However, the underlying molecular properties remain unclear. In this research, we performed RNA-Seq to identify differences in the gene expression between surgical bAVM tissues from the HFR group and the LFR group and to facilitate the understanding of the molecular mechanisms in bAVMs with different flow rates. We identified FZD10 and MYOC in vascular ECs and SMCs as key molecules, and Wnt signaling was activated in the LFR group patients. The function of FZD10 and MYOC was investigated in cultured ECs and SMCs. We found that overexpression of the 2 molecules could activate canonical Wnt signaling to promote angiogenesis responses, such as cell migration and tube formation, which might induce high resistance and lead to phenotypes of low blood flow rate.

A previous study based on microarray analysis identified several neuron-related genes, including NPY, SYT1, NeuroD, and EFNB3, which were downregulated in the HFR bAVMs.[12] This result explained only the neuronal network injury caused by the lack of perfusion in the perinidal area, which might be the outcome rather than the cause of high blood flow rate.[23] In our study, RNA-Seq data and functional pathway analysis suggested that FZD10 and MYOC had relatively high expression levels in LFR bAVMs. They were involved in the activation of Wnt signaling, which plays important roles in central nervous system angiogenesis and regulates vessel density during embryonic development.[16,24–26] In cultured ECs and SMCs, we found that overexpressed FZD10 and MYOC could activate canonical rather than noncanonical Wnt signaling, which was consistent with a previous study.[17,20] We postulated

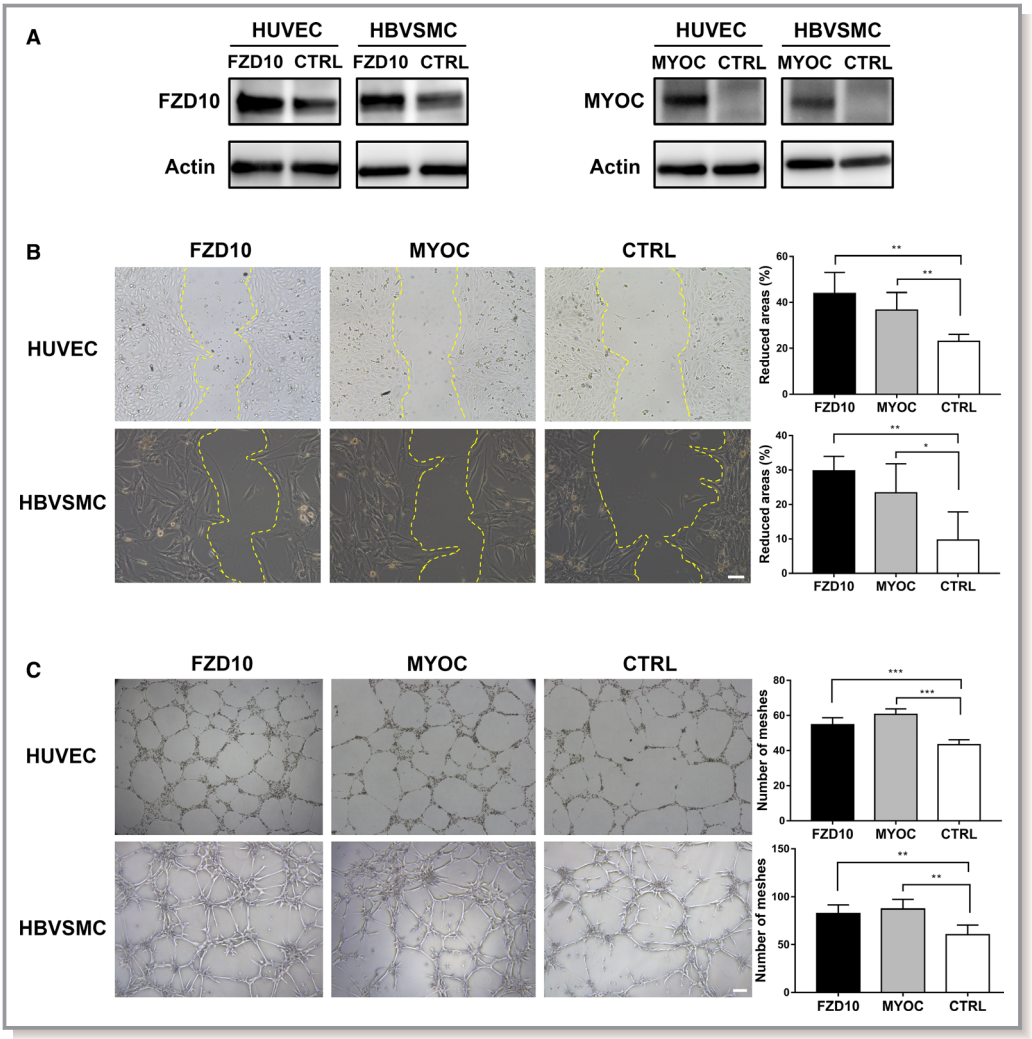

Figure 4. Effects of FZD10 and MYOC on HUVECs and HBVSMCs. **A**, Western blotting analysis of HUVECs and HBVSMCs transfected with a pcDNA3 vector overexpressing FZD10/MYOC or negative control (CTRL). **B**, Effects of FZD10/MYOC on migration of HUVECs and HBVSMCs. The scale bar corresponds to 100 μm. **C**, Effects of FZD10/MYOC on tube formation of HUVECs and HBVSMCs. The scale bar corresponds to 200 μm. One representative experiment out of 5 is shown. **P*<0.05; ***P*<0.025; ****P*<0.001. HBVSMCs indicates human brain vascular smooth muscle cells; HUVECs, human umbilical vein endothelial cells.

that the upregulation of canonical Wnt signaling might increase the blood vessel density of bAVMs, eventually resulting in an increase in vascular resistance and a reduction in blood flow rate. Our study implies that targeting FZD10, MYOC, and canonical Wnt signaling might modulate the blood flow rate in bAVMs.

The morphologic and functional changes in vascular ECs and SMCs are involved in the pathophysiological process of bAVMs.[27,28] Whole-exome sequencing of bAVMs showed that some vascular ECs contained KRAS mutations, and further investigation revealed that cultured ECs that had the same mutation were phenotypically larger and elongated, demonstrated faster migration, and had more cytoskeletal actin projections.[29] SMCs derived from bAVMs formed tubes in culture, which were longer than those formed by normal brain vascular SMCs. The migration and proliferation of bAVM SMCs also exceeded those of normal brain vascular SMCs.[30] These findings suggest that the pathogenesis of bAVMs is likely because of abnormal vascular ECs and SMCs. Whether the function of vascular ECs and SMCs affects the phenotype development of bAVMs is still unknown. In this study, we observed that overexpressed FZD10 and MYOC were mainly concentrated in vascular ECs and SMCs of LFR bAVMs. In vitro experiments further verified that overexpression of FZD10 and MYOC improved the migration and tube formation of ECs and SMCs. These results suggested that ECs and SMCs might play essential roles in the regulation of different flow rate phenotype development in bAVMs as well.

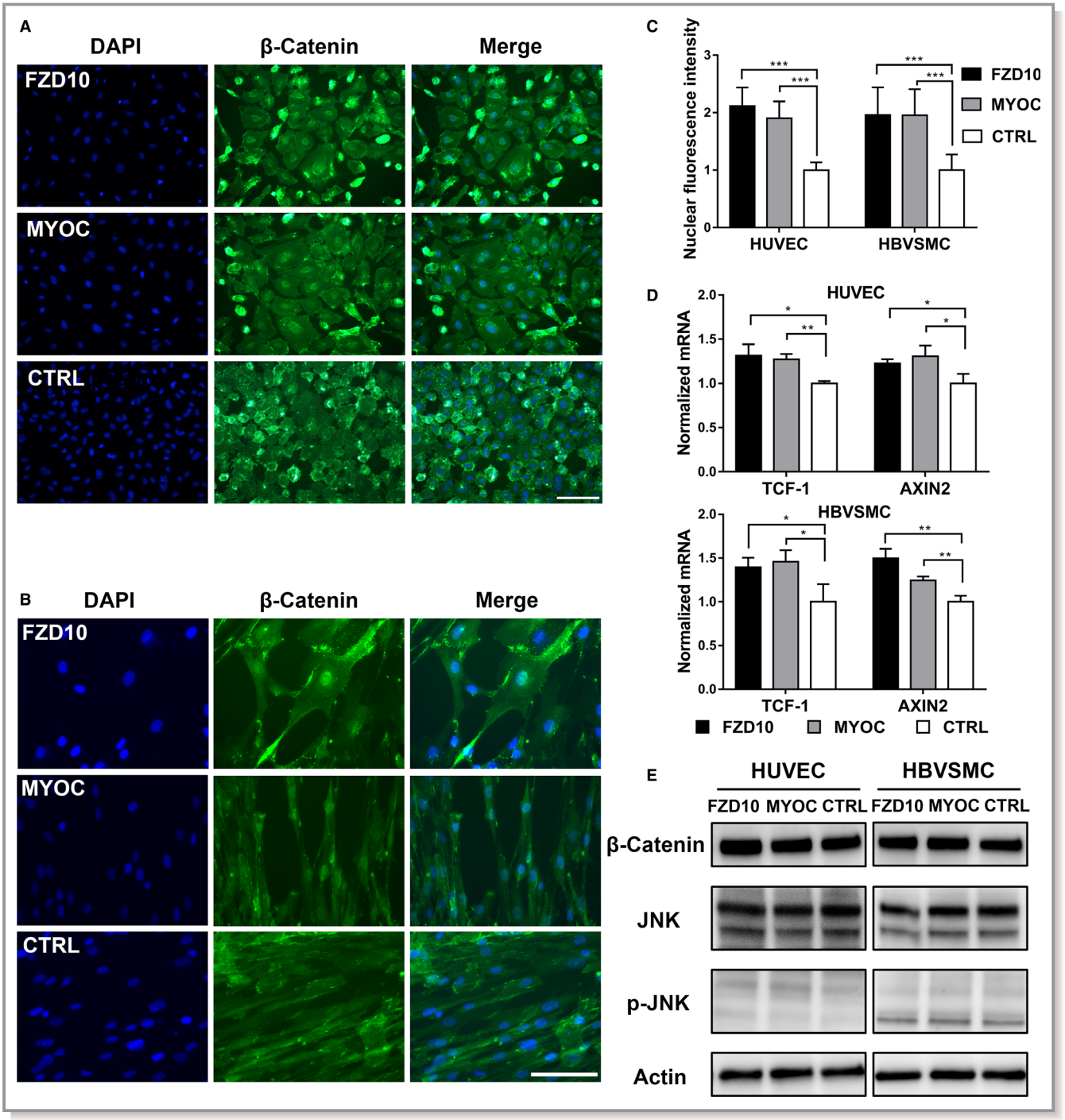

Figure 5. Wnt signaling is influenced by FZD10 or MYOC in HUVECs and HBVSMCs. Immunofluorescent staining for β-catenin in HUVECs (**A**) and HBVSMCs (**B**) transfected with a pcDNA3 vector overexpressing FZD10/MYOC or negative control (CTRL). **C**, Nuclear β-catenin level was quantified by measuring fluorescence intensity in the cell nucleus. Data were derived from 3 randomly selected fields. **D**, RT-qPCR for AXIN2 and TCF-1 expression in HUVECs and HBVSMCs transfected as in (**A**, **B**). **E**, Western blotting analysis for total JNK (t-JNK), p-JNK (Thr183/Tyr185), and β-catenin in HUVECs and HBVSMCs transfected as in (**A**, **B**). **P*<0.05; ***P*<0.025; ****P*<0.001. The scale bar corresponds to 200 μm. These data are representative of 3 independent experiments. DAPI indicates 4′,6-diamidino-2-phenylindole; HBVSMCs, human brain vascular smooth muscle cells; RT-qPCR, reverse transcription quantitative polymerase chain reaction; HUVECs, human umbilical vein endothelial cells.

Currently, clinical decisions for bAVMs are still in a dilemma, particularly when dealing with certain difficult cases, such as large bAVMs located near or in the functional areas.[31,32] Alternative novel therapeutic strategies with higher safety and efficacy need to be explored. The blood flow rate of bAVMs, which is an important factor that has a relationship

with prognosis, could be a potential target for intervention. By performing RNA-Seq on bAVM tissues dissected from patients, we found differential gene expression profiling between bAVMs with different flow rates, providing a potential therapeutic target to regulate the blood flow rate, which might provide a promising perspective for bAVM treatment.

Acknowledgments

We thank Zhicen Li and Ji Ma for their contributions to the data collection. We also thank Yang Liu, Jiayu Li, and Haoyu Li for their assistance in manuscript preparation.

Sources of Funding

This study was supported by the "National Key Research and Development Program of China during the 13th Five-Year Plan Period" (Grant No. 2016YFC1301803, Principle Investigator: Professor Yong Cao and Grant No. 2016YFC1301801, Principle Investigator: Professor Shuo Wang) and the "Key Project of Beijing Municipal Science & Technology Commission" (Grant No. D161100003816006, Principal Investigator: Professor Shuo Wang and Grant No. D161100003816005, Principle Investigator: Professor Jizong Zhao).

Disclosures

None.

References

1. Solomon RA, Connolly ES. Arteriovenous malformations of the brain. *N Engl J Med*. 2017;376:1859–1866.
2. Fullerton HJ, Achrol AS, Johnston SC, McCulloch CE, Higashida RT, Lawton MT, Sidney S, Young WL. Long-term hemorrhage risk in children versus adults with brain arteriovenous malformations. *Stroke*. 2005;36:2099–2104.
3. Meyer-Heim AD, Boltshauser E. Spontaneous intracranial haemorrhage in children: aetiology, presentation and outcome. *Brain Dev*. 2003;25:416–421.
4. Derdeyn CP, Zipfel GJ, Albuquerque FC, Cooke DL, Feldmann E, Sheehan JP, Torner JC. Management of brain arteriovenous malformations: a scientific statement for healthcare professionals from the American Heart Association/American Stroke Association. *Stroke*. 2017;48:e200–e224.
5. Mohr JP, Parides MK, Stapf C, Moquete E, Moy CS, Overbey JR, Al-Shahi SR, Vicaut E, Young WL, Houdart E, Cordonnier C, Stefani MA, Hartmann A, von Kummer R, Biondi A, Berkefeld J, Klijn CJ, Harkness K, Libman R, Barreau X, Moskowitz AJ. Medical management with or without interventional therapy for unruptured brain arteriovenous malformations (Aruba): a multicentre, non-blinded, randomised trial. *Lancet*. 2014;383:614–621.
6. Chen X, Cooke DL, Saloner D, Nelson J, Su H, Lawton MT, Hess C, Tihan T, Zhao Y, Kim H. Higher flow is present in unruptured arteriovenous malformations with silent intralesional microhemorrhages. *Stroke*. 2017;48:2881–2884.
7. Taeshineetanakul P, Krings T, Geibprasert S, Menezes R, Agid R, Terbrugge KG, Schwartz ML. Angioarchitecture determines obliteration rate after radiosurgery in brain arteriovenous malformations. *Neurosurgery*. 2012;71:1071–1078; discussion 1079.
8. Rangel-Castilla L, Spetzler RF, Nakaji P. Normal perfusion pressure breakthrough theory: a reappraisal after 35 years. *Neurosurg Rev*. 2015;38:399–404:discussion 404–5.
9. Ma L, Chen XL, Chen Y, Wu CX, Ma J, Zhao YL. Subsequent haemorrhage in children with untreated brain arteriovenous malformation: higher risk with unbalanced inflow and outflow angioarchitecture. *Eur Radiol*. 2017;27:2868–2876.
10. Fukuoka S, Takanashi M, Seo Y, Suematsu K, Nakamura J. Radiosurgery for arteriovenous malformations with gamma-knife: a multivariate analysis of factors influencing the complete obliteration rate. *J Clin Neurosci*. 1998;5 (suppl):68–71.
11. Weinsheimer SM, Xu H, Achrol AS, Stamova B, McCulloch CE, Pawlikowska L, Tian Y, Ko NU, Lawton MT, Steinberg GK, Chang SD, Jickling G, Ander BP, Kim H, Sharp FR, Young WL. Gene expression profiling of blood in brain arteriovenous malformation patients. *Transl Stroke Res*. 2011;2:575–587.
12. Takagi Y, Aoki T, Takahashi JC, Yoshida K, Ishii A, Arakawa Y, Kikuchi T, Funaki T, Miyamoto S. Differential gene expression in relation to the clinical characteristics of human brain arteriovenous malformations. *Neurol Med Chir*. 2014;54:163–175.
13. 't Hoen PA, Ariyurek Y, Thygesen HH, Vreugdenhil E, Vossen RH, de Menezes RX, Boer JM, van Ommen GJ, den Dunnen JT. Deep sequencing-based expression analysis shows major advances in robustness, resolution and inter-lab portability over five microarray platforms. *Nucleic Acids Res*. 2008;36:e141.
14. Shovlin CL, Guttmacher AE, Buscarini E, Faughnan ME, Hyland RH, Westermann CJ, Kjeldsen AD, Plauchu H. Diagnostic criteria for hereditary hemorrhagic telangiectasia (rendu-osler-weber syndrome). *Am J Med Genet*. 2000;91:66–67.
15. Hermanto Y, Takagi Y, Ishii A, Yoshida K, Kikuchi T, Funaki T, Mineharu Y, Miyamoto S. Immunohistochemical analysis Sox17 associated pathway in brain arteriovenous malformations. *World Neurosurg*. 2015;87:573–583.
16. Corada M, Nyqvist D, Orsenigo F, Caprini A, Giampietro C, Taketo MM, Iruela-Arispe ML, Adams RH, Dejana E. The Wnt/beta-catenin pathway modulates vascular remodeling and specification by upregulating D114/notch signaling. *Dev Cell*. 2010;18:938–949.
17. Gong C, Qu S, Lv XB, Liu B, Tan W, Nie Y, Su F, Liu Q, Yao H, Song E. BRMS1L suppresses breast cancer metastasis by inducing epigenetic silence of FZD10. *Nat Commun*. 2014;5:5406.
18. Fukukawa C, Nagayama S, Tsunoda T, Toguchida J, Nakamura Y, Katagiri T. Activation of the non-canonical Dvl-Rac1-JNK pathway by frizzled homologue 10 in human synovial sarcoma. *Oncogene*. 2009;28:1110–1120.
19. Kwon HS, Lee HS, Ji Y, Rubin JS, Tomarev SI. Myocilin is a modulator of Wnt signaling. *Mol Cell Biol*. 2009;29:2139–2154.
20. Shen X, Ying H, Yue BY. Wnt activation by wild type and mutant myocilin in cultured human trabecular meshwork cells. *PLoS One*. 2012;7:e44902.
21. Hot B, Valnohova J, Arthofer E, Simon K, Shin J, Uhlen M, Kostenis E, Mulder J, Schulte G. FZD_{10}-$G\alpha_{13}$ signalling axis points to a role of FZD10 in CNS angiogenesis. *Cell Signal*. 2017;32:93–103.
22. Kwon HS, Tomarev SI. Myocilin, a glaucoma-associated protein, promotes cell migration through activation of integrin-focal adhesion kinase-serine/threonine kinase signaling pathway. *J Cell Physiol*. 2011;226:3392–3402.
23. Takagi Y, Kikuta K, Nozaki K, Fujimoto M, Hayashi J, Hashimoto N. Neuronal expression of Fas-associated death domain protein and caspase-8 in the perinidal parenchyma of cerebral arteriovenous malformations. *J Neurosurg*. 2007;106:275–282.
24. Tata M, Ruhrberg C, Fantin A. Vascularisation of the central nervous system. *Mech Dev*. 2015;138:26–36.
25. Corada M, Morini MF, Dejana E. Signaling pathways in the specification of arteries and veins. *Arterioscler Thromb Vasc Biol*. 2014;34:2372–2377.
26. Phng LK, Potente M, Leslie JD, Babbage J, Nyqvist D, Lobov I, Ondr JK, Rao S, Lang RA, Thurston G, Gerhardt H. Nrarp coordinates endothelial Notch and Wnt signaling to control vessel density in angiogenesis. *Dev Cell*. 2009;16:70–82.
27. Crist AM, Lee AR, Patel NR, Westhoff DE, Meadows SM. Vascular deficiency of Smad4 causes arteriovenous malformations: a mouse model of hereditary hemorrhagic telangiectasia. *Angiogenesis*. 2018;21:363–380.
28. Frösen J, Joutel A. Smooth muscle cells of intracranial vessels: from development to disease. *Cardiovasc Res*. 2018;114:501–512.
29. Nikolaev SI, Vetiska S, Bonilla X, Boudreau E, Jauhiainen S, Jahromi BR, Khyzha N, DiStefano PV, Suutarinen S, Kiehl TR, Pereira VM, Herman AM, Krings T, Andrade-Barazarte H, Tung T, Valiante T, Zadeh G, Tymianski M, Rauramaa T, Ylä-Herttuala S, Wythe JD, Antonarakis SE, Frösen J, Fish JE, Radovanovic I. Somatic activating kRAS mutations in arteriovenous malformations of the brain. *N Engl J Med*. 2018;378:250–261.
30. Huang J, Song J, Qu M, Wang Y, An Q, Song Y, Yan W, Wang B, Wang X, Zhang S, Chen X, Zhao B, Liu P, Xu T, Zhang Z, Greenberg DA, Wang Y, Gao P, Zhu W, Yang GY. MicrorRNA-137 and microrNA-195* inhibit vasculogenesis in brain arteriovenous malformations. *Ann Neurol*. 2017;82:371–384.
31. Lawton MT; UCSF Brain Arteriovenous Malformation Study Project. Spetzler-Martin Grade III arteriovenous malformations: surgical results and a modification of the grading scale. *Neurosurgery*. 2003;52:740–748: discussion 748–749.
32. Reinard KA, Pabaney AH, Basheer A, Phillips SB, Kole MK, Malik GM. Surgical management of giant intracranial arteriovenous malformations: a single center experience over 32 years. *World Neurosurg*. 2015;84:1765–1778.

SUPPLEMENTAL MATERIAL

Data S1.

Supplemental Methods

Immunofluorescence

For immunofluorescent staining, transfected HUVECs and HBVSMCs were fixed in paraformaldehyde. After permeabilization in 0.2% Triton X-100 and blocking, the cells were incubated with primary antibodies against β-catenin (1:250, ab32572, Abcam) overnight at 4°C and then incubated with an Alexa Fluor 488-conjugated goat antibody against rabbit (1:200, ab150077, Abcam) at room temperature for 1 h. Finally, the cells were counterstained with 4,6-diamidino-2-phenylindole and imaged using an EVOS™ FL Auto 2 Imaging System (Invitrogen).

Western blotting

Whole-cell lysates were prepared using RIPA buffer. Equal amounts of total protein (20 μg) from cell lysates were loaded on a 10% SDS/PAGE gel, transferred to a PVDF membrane (Millipore), and detected using a BOX F3 Gel Documentation System (Syngene). The primary antibodies used were as follows: FZD10 (1:1000, NBP2-23659SS, Novus), MYOC (1:500, MAB3446, R&D), β-catenin (1:4000, ab32572, Abcam), JNK (1:1000, 9252S, CST) and p-JNK (1:1000, Thr183/Tyr185, 81E11, CST). β-actin (1:2000, P30002M, Abmart) was used as the

loading control. The secondary antibodies used were goat anti-rabbit (1:3000, M21002, Abmart) and goat anti-mouse (1:3000, M21001, Abmart) IgG-HRP.

Wound healing assay

Wound healing assays were performed with an Ibidi Culture-Insert (Ibidi). Briefly, transfected cells were seeded into the wells to obtain a confluent layer. After appropriate cell attachment, the Culture-Insert was gently removed using sterile tweezers. Then, the well was filled with serum-free medium to exclude the effect of cell proliferation. The percentage of the reduced area was measured at 48 h post-transfection with NIH ImageJ software.

Tube formation assay

Ibidi μ-Slide Angiogenesis (Ibidi) was used to perform tube formation assays with HUVECs and HBVSMCs. Briefly, 48 h after transfection, cells were seeded on Matrigel (BD Inc., San Jose, CA, US) in the wells of the Slides. After the formation of tube structures, the number of meshes was measured and quantified.

Proliferation assay

Briefly, cells (1×10^4 cells/well) were seeded in 96-well plates with 100 μL of medium per well. Cell Counting Kit-8 solution (Dojindo Laboratories, Kumamoto, Japan) was added to the cell culture medium to a final concentration of 5 μL/100 μL and incubated for an additional 3 h

at 37°C. The absorbance at 450 nm was measured using a microplate reader (Molecular Devices).

Table S1. Primers used for RT-qPCR.

Primers for genes	Sequence
FZD10-F	TATCGGGCTCTTCTCTGTGC
FZD10-R	GACTGGGCAGGGATCTCATA
MYOC-F	ATCTCAGGAGTGGAGAGGGA
MYOC-R	CTGGCTGATGAGGTCATACTC
AXIN2-F	AGTGTGAGGTCCACGGAAAC
AXIN2-R	CTGGTGCAAAGACATAGCCA
TCF-1-F	AGGAGATGAGAGCCAAGGTCA
TCF-1-R	AGCCTGGGTATAGCTGCATGT
GAPDH-F	AATGACCCCTTCATTGAC
GAPDH-R	TCCACGACGTACTCAGCGC

Table S2. Differential expression profile.

Ensembl ID	Gene symbol	FPKM (LFR)	FPKM (HFR)	FC	P value
ENSG00000198812.3	LRRC10	0.036	0.006	6.338	7.41E-06
ENSG00000120833.9	SOCS2	16.421	7.754	2.118	1.46E-05
ENSG00000223516.1	AFF2-IT1	0.288	0.040	7.196	4.89E-05
ENSG00000183888.4	C1orf64	2.004	0.933	2.149	5.19E-05
ENSG00000204950.2	LRRC10B	4.075	1.551	2.628	6.55E-05
ENSG00000167034.9	NKX3-1	1.892	0.767	2.467	7.85E-05
ENSG00000111432.4	FZD10	1.935	0.726	2.667	0.000112
ENSG00000133665.8	DYDC2	0.473	0.157	3.010	0.000124
ENSG00000244040.1	IL12A-AS1	0.147	0.060	2.446	0.00014
ENSG00000185022.7	MAFF	42.090	19.994	2.105	0.000164
ENSG00000108342.8	CSF3	9.461	1.070	8.842	0.000169
ENSG00000172602.5	RND1	23.382	9.117	2.565	0.000211
ENSG00000034971.10	MYOC	0.329	0.067	4.895	0.000237
ENSG00000197826.7	C4orf22	0.416	0.049	8.434	0.000252
ENSG00000231274.4	SBK3	0.136	0.014	9.535	0.000347
ENSG00000171124.8	FUT3	0.064	0.011	5.928	0.000403
ENSG00000180616.4	SSTR2	9.698	4.829	2.008	0.000489
ENSG00000228002.2	DHX9P1	0.049	0.014	3.424	0.000525
ENSG00000268654.1	MIMT1	0.420	0.141	2.987	0.000711
ENSG00000130164.7	LDLR	45.012	21.491	2.094	0.000761
ENSG00000199218.1	RN7SKP184	1.105	0.400	2.762	0.000798
ENSG00000137699.12	TRIM29	0.633	0.216	2.934	0.00086
ENSG00000213612.3	FAM220CP	0.867	0.377	2.300	0.000889
ENSG00000100078.3	PLA2G3	0.060	0.014	4.181	0.001184
ENSG00000142973.8	CYP4B1	0.514	0.095	5.405	0.001186
ENSG00000244112.2	RN7SL508P	1.858	0.501	3.710	0.001364
ENSG00000235631.1	RNF148	1.429	0.700	2.042	0.001417
ENSG00000164736.5	SOX17	9.911	4.394	2.256	0.001599
ENSG00000147869.4	CER1	0.122	0.037	3.274	0.001648
ENSG00000228670.4	NANOGP2	0.471	0.184	2.565	0.001669
ENSG00000115602.12	IL1RL1	11.498	3.403	3.379	0.001871
ENSG00000101187.11	SLCO4A1	6.244	2.778	2.248	0.001963
ENSG00000134398.8	ERN2	0.099	0.027	3.664	0.00215
ENSG00000271723.1	MROH7-TTC4	0.873	0.414	2.108	0.002176
ENSG00000232354.3	VIPR1-AS1	0.494	0.238	2.075	0.002255

ENSG00000007908.11	SELE	53.814	19.319	2.786	0.002313
ENSG00000117595.6	IRF6	2.576	1.140	2.259	0.002518
ENSG00000116176.6	TPSG1	0.162	0.065	2.491	0.002607
ENSG00000057593.9	F7	0.462	0.205	2.256	0.002872
ENSG00000171873.6	ADRA1D	0.593	0.296	2.000	0.003027
ENSG00000229268.1	PES1P2	0.185	0.084	2.209	0.003077
ENSG00000165269.8	AQP7	0.315	0.132	2.385	0.003103
ENSG00000198535.5	C2CD4A	0.895	0.144	6.200	0.003158
ENSG00000137225.8	CAPN11	0.112	0.271	0.413	0.003262
ENSG00000257482.3	ZNF727	0.663	0.310	2.139	0.003354
ENSG00000158055.11	GRHL3	0.853	0.393	2.171	0.003587
ENSG00000164142.11	FAM160A1	0.939	0.349	2.687	0.003625
ENSG00000175592.4	FOSL1	17.211	7.112	2.420	0.003666
ENSG00000104369.4	JPH1	3.205	1.446	2.216	0.00376
ENSG00000177182.6	CLVS1	2.702	1.325	2.039	0.003943
ENSG00000154864.7	PIEZO2	4.403	8.821	0.499	0.004084
ENSG00000146674.10	IGFBP3	75.574	36.226	2.086	0.004172
ENSG00000130037.3	KCNA5	7.247	3.254	2.227	0.004236
ENSG00000267206.1	LCN6	1.904	0.926	2.056	0.004536
ENSG00000234373.1	SNX18P7	0.766	0.175	4.377	0.004598
ENSG00000127530.2	OR7C1	0.168	0.066	2.562	0.00464
ENSG00000174567.7	GOLT1A	0.269	0.081	3.299	0.004671
ENSG00000241890.1	RPL13P4	0.283	0.088	3.224	0.00474
ENSG00000180440.3	SERTM1	2.006	0.753	2.664	0.004994
ENSG00000181577.11	C6orf223	0.422	0.205	2.061	0.00529
ENSG00000149735.2	GPHA2	0.346	0.155	2.235	0.005382
ENSG00000086544.2	ITPKC	16.885	7.662	2.204	0.005402
ENSG00000206199.5	ANKUB1	0.528	1.083	0.487	0.005797
ENSG00000086717.14	PPEF1	0.781	0.382	2.043	0.005863
ENSG00000125144.9	MT1G	59.161	28.311	2.090	0.005964
ENSG00000149305.2	HTR3B	0.863	0.301	2.871	0.00632
ENSG00000256977.6	LIMS3	1.790	0.522	3.428	0.006417
ENSG00000205177.5	C11orf91	3.039	1.170	2.598	0.006421
ENSG00000272636.1	DOC2B	6.229	3.054	2.040	0.006435
ENSG00000224551.1	HMGB3P21	0.174	0.476	0.364	0.006437
ENSG00000172987.8	HPSE2	0.704	0.290	2.427	0.006449
ENSG00000136244.7	IL6	129.305	40.561	3.188	0.006634
ENSG00000137251.11	TINAG	0.084	0.022	3.772	0.006641
ENSG00000171056.6	SOX7	8.044	3.779	2.128	0.006691

ENSG00000172995.12	ARPP21	33.612	16.146	2.082	0.006779
ENSG00000156427.7	FGF18	2.521	1.061	2.375	0.006899
ENSG00000124249.5	KCNK15	1.340	0.617	2.171	0.007017
ENSG00000205502.3	C2CD4B	17.177	5.054	3.399	0.007036
ENSG00000160963.9	COL26A1	2.743	1.311	2.093	0.007248
ENSG00000257302.1	FAHD2P1	0.372	0.115	3.231	0.007249
ENSG00000256391.1	SDIM1	0.554	0.206	2.681	0.007385
ENSG00000174482.6	LINGO2	2.772	1.319	2.101	0.00746
ENSG00000237990.2	CNTN4-AS1	0.250	0.108	2.320	0.007565
ENSG00000187479.4	C11orf96	219.261	100.593	2.180	0.007604
ENSG00000226627.1	SHANK2-AS1	0.614	0.300	2.046	0.007605
ENSG00000229417.1	NPM1P25	0.446	0.958	0.466	0.007795
ENSG00000121446.13	RGSL1	0.013	0.004	3.027	0.007928
ENSG00000141433.8	ADCYAP1	3.499	0.871	4.018	0.008021
ENSG00000053438.7	NNAT	25.518	10.636	2.399	0.008035
ENSG00000258392.1	RPA2P1	0.261	0.117	2.226	0.008127
ENSG00000264315.1	HNRNPA1P11	1.133	0.342	3.312	0.008148
ENSG00000254244.1	PAICSP4	1.582	0.682	2.319	0.008468
ENSG00000183729.3	NPBWR1	0.122	0.042	2.886	0.008484
ENSG00000237665.1	GRM7-AS2	0.975	0.243	4.015	0.008604
ENSG00000229975.1	LIPT1P1	0.804	0.354	2.269	0.008689
ENSG00000143333.6	RGS16	28.924	13.181	2.194	0.008781
ENSG00000121742.11	GJB6	7.545	3.026	2.493	0.009014
ENSG00000136883.8	KIF12	0.479	0.187	2.558	0.00905
ENSG00000255277.2	ABCC6P2	0.234	0.111	2.096	0.009177
ENSG00000140968.6	IRF8	11.845	25.039	0.473	0.009297
ENSG00000176697.14	BDNF	2.186	0.871	2.508	0.009474
ENSG00000145040.3	UCN2	1.194	0.524	2.276	0.009507
ENSG00000224683.1	RPL36AP29	0.550	0.178	3.092	0.009523
ENSG00000183036.6	PCP4	9.836	4.837	2.033	0.009578
ENSG00000132510.6	KDM6B	65.547	32.118	2.041	0.009782
ENSG00000130368.4	MAS1	0.762	0.278	2.742	0.009861
ENSG00000188817.3	SNTN	0.082	0.035	2.347	0.009937
ENSG00000120280.5	CXorf21	2.545	5.396	0.472	0.009988
ENSG00000188282.8	RUFY4	0.288	0.678	0.425	0.010029
ENSG00000168334.8	XIRP1	1.756	0.561	3.128	0.010062
ENSG00000266274.1	RN7SL138P	8.730	21.470	0.407	0.010375
ENSG00000103196.7	CRISPLD2	76.349	36.091	2.115	0.010533
ENSG00000213450.4	VDAC1P7	0.182	0.062	2.927	0.010617

ENSG00000167772.7	ANGPTL4	16.794	8.347	2.012	0.010703
ENSG00000226981.2	ABHD17AP6	0.404	0.103	3.926	0.01083
ENSG00000171643.9	S100Z	0.178	0.495	0.360	0.010835
ENSG00000143627.13	PKLR	0.079	0.029	2.704	0.011001
ENSG00000264668.1	ZFP41	0.519	0.241	2.158	0.011084
ENSG00000103154.5	NECAB2	10.238	4.693	2.182	0.011159
ENSG00000179639.6	FCER1A	1.410	2.904	0.486	0.011223
ENSG00000110680.8	CALCA	0.480	0.149	3.215	0.011261
ENSG00000157502.8	MUM1L1	0.924	0.440	2.100	0.011372
ENSG00000136997.10	MYC	54.727	26.951	2.031	0.011519
ENSG00000188522.10	FAM83G	2.543	1.141	2.228	0.011593
ENSG00000261429.2	DPPA2P4	0.421	0.135	3.119	0.011595
ENSG00000129451.7	KLK10	0.211	0.065	3.239	0.01165
ENSG00000010319.2	SEMA3G	13.011	6.071	2.143	0.011757
ENSG00000229001.1	ACTBP14	0.111	0.052	2.136	0.011815
ENSG00000198576.2	ARC	23.119	7.884	2.932	0.011908
ENSG00000101204.11	CHRNA4	2.483	1.186	2.093	0.011911
ENSG00000183186.6	C2CD4C	3.168	1.370	2.312	0.01208
ENSG00000172818.5	OVOL1	0.175	0.059	2.959	0.012181
ENSG00000235280.2	MCF2L-AS1	0.306	0.135	2.268	0.012291
ENSG00000149380.7	P4HA3	0.993	2.229	0.446	0.012513
ENSG00000244752.2	CRYBB2	0.185	0.091	2.025	0.01252
ENSG00000178394.3	HTR1A	2.163	0.906	2.388	0.01261
ENSG00000095752.2	IL11	1.019	0.373	2.732	0.012832
ENSG00000116544.7	DLGAP3	18.073	8.741	2.068	0.013064
ENSG00000181418.7	DDN	25.821	11.666	2.213	0.013537
ENSG00000137825.6	ITPKA	8.021	3.359	2.388	0.013837
ENSG00000139865.12	TTC6	0.261	0.105	2.481	0.013882
ENSG00000184908.13	CLCNKB	0.151	0.063	2.395	0.013972
ENSG00000138316.6	ADAMTS14	0.742	1.821	0.407	0.014085
ENSG00000111247.10	RAD51AP1	1.131	2.484	0.455	0.014337
ENSG00000233123.1	LINC01007	1.620	0.329	4.930	0.014378
ENSG00000128342.4	LIF	32.215	11.834	2.722	0.014481
ENSG00000124664.6	SPDEF	0.227	0.099	2.289	0.014839
ENSG00000271108.1	KATNBL1P5	0.203	0.645	0.315	0.015181
ENSG00000143228.8	NUF2	0.494	1.236	0.400	0.0154
ENSG00000149654.5	CDH22	4.936	2.270	2.175	0.015578
ENSG00000188959.9	C9orf152	0.115	0.049	2.370	0.016061
ENSG00000225101.3	OR52K3P	0.391	0.881	0.443	0.01636

ENSG00000177508.11	IRX3	2.102	0.927	2.268	0.016441
ENSG00000105509.6	HAS1	3.376	1.368	2.468	0.016618
ENSG00000184601.6	C14orf180	0.416	0.196	2.119	0.016819
ENSG00000144550.8	CPNE9	1.875	0.851	2.202	0.016827
ENSG00000166823.5	MESP1	1.135	0.555	2.045	0.017257
ENSG00000226510.1	UPK1A-AS1	0.135	0.057	2.360	0.017289
ENSG00000144119.3	C1QL2	1.780	0.721	2.468	0.017418
ENSG00000118017.3	A4GNT	0.045	0.124	0.359	0.017737
ENSG00000251449.2	MTND1P19	2.828	0.902	3.135	0.017775
ENSG00000143340.6	FAM163A	0.309	0.093	3.327	0.017798
ENSG00000071282.7	LMCD1	67.751	30.796	2.200	0.017922
ENSG00000123219.8	CENPK	1.367	2.982	0.458	0.018003
ENSG00000189181.3	OR14I1	0.709	0.251	2.829	0.018163
ENSG00000263878.1	DLGAP1-AS4	2.446	1.070	2.286	0.018291
ENSG00000134551.8	PRH2	0.325	0.659	0.493	0.018548
ENSG00000239794.2	RN7SL653P	1.805	0.863	2.092	0.01859
ENSG00000105492.11	SIGLEC6	0.144	0.402	0.358	0.018599
ENSG00000089558.4	KCNH4	0.737	0.331	2.229	0.018821
ENSG00000168634.4	WFDC13	0.086	0.034	2.552	0.018962
ENSG00000173714.7	WFIKKN2	1.109	0.369	3.004	0.018964
ENSG00000105383.10	CD33	3.986	8.132	0.490	0.019101
ENSG00000241295.1	ZBTB20-AS2	0.534	1.524	0.350	0.019237
ENSG00000205358.3	MT1H	8.658	3.946	2.194	0.019397
ENSG00000126583.6	PRKCG	7.575	3.316	2.284	0.019407
ENSG00000265264.1	TIMM10B	0.357	0.128	2.795	0.019473
ENSG00000255734.1	HNRNPABP1	0.066	0.199	0.331	0.019511
ENSG00000220868.2	MRPL35P1	0.341	0.156	2.192	0.019618
ENSG00000175793.10	SFN	0.784	0.342	2.292	0.019672
ENSG00000198153.7	ZNF849P	0.063	0.024	2.593	0.019934
ENSG00000197901.7	SLC22A6	4.578	1.076	4.256	0.019936
ENSG00000171954.8	CYP4F22	0.025	0.074	0.345	0.020205
ENSG00000233642.1	GPR158-AS1	0.100	0.049	2.029	0.020424
ENSG00000101280.6	ANGPT4	1.011	0.502	2.014	0.020446
ENSG00000183856.6	IQGAP3	0.352	0.866	0.407	0.020525
ENSG00000235489.3	DBF4P1	0.141	0.055	2.555	0.020528
ENSG00000162510.5	MATN1	0.234	0.109	2.139	0.020957
ENSG00000230539.1	AOAH-IT1	0.239	0.529	0.451	0.021147
ENSG00000256193.1	LINC00507	2.060	0.721	2.858	0.021506
ENSG00000196946.5	ZNF705A	0.052	0.011	4.818	0.021808

ENSG00000184185.5	KCNJ12	1.818	0.802	2.266	0.021884
ENSG00000120093.7	HOXB3	0.341	0.784	0.434	0.021909
ENSG00000151117.4	TMEM86A	3.267	6.651	0.491	0.02197
ENSG00000227766.1	HCG4P5	0.915	2.096	0.437	0.022002
ENSG00000268849.1	SIGLEC22P	0.564	1.187	0.475	0.022127
ENSG00000123338.8	NCKAP1L	12.876	26.771	0.481	0.0224
ENSG00000187094.7	CCK	38.377	17.314	2.217	0.022716
ENSG00000152430.13	BOLL	0.102	0.223	0.460	0.022842
ENSG00000225781.1	OR6V1	0.208	0.518	0.402	0.022859
ENSG00000229570.2	GAPDHP58	0.206	0.074	2.776	0.022971
ENSG00000147571.3	CRH	0.750	0.301	2.493	0.022987
ENSG00000249206.2	GCNT1P2	0.256	0.109	2.362	0.023202
ENSG00000188985.5	DHFRP1	0.092	0.035	2.618	0.023241
ENSG00000237575.4	PYY2	0.154	0.337	0.457	0.023647
ENSG00000182048.7	TRPC2	0.124	0.286	0.434	0.023745
ENSG00000258956.2	COX4I1P1	0.382	0.164	2.338	0.02391
ENSG00000161640.11	SIGLEC11	0.788	1.637	0.482	0.024011
ENSG00000232901.1	CYCSP10	0.667	1.406	0.474	0.024067
ENSG00000132671.4	SSTR4	0.268	0.121	2.217	0.024373
ENSG00000184060.6	ADAP2	13.831	28.044	0.493	0.024495
ENSG00000221890.2	NPTXR	31.510	13.989	2.253	0.024516
ENSG00000106236.3	NPTX2	17.779	5.529	3.215	0.025088
ENSG00000100122.5	CRYBB1	0.879	1.986	0.443	0.025235
ENSG00000230453.5	ANKRD18B	1.349	0.525	2.570	0.025815
ENSG00000089169.10	RPH3A	19.873	8.988	2.211	0.025923
ENSG00000240014.2	RN7SL254P	1.003	0.464	2.163	0.026169
ENSG00000095970.12	TREM2	18.718	41.030	0.456	0.026339
ENSG00000242285.1	RPL6P8	0.082	0.221	0.370	0.02634
ENSG00000158488.11	CD1E	0.330	0.674	0.490	0.026659
ENSG00000138413.9	IDH1	16.933	41.071	0.412	0.026738
ENSG00000253974.1	NRG1-IT1	0.821	0.378	2.173	0.026848
ENSG00000243547.1	HNRNPKP4	0.048	0.021	2.322	0.027674
ENSG00000156970.8	BUB1B	0.706	1.780	0.397	0.027833
ENSG00000225079.2	FTH1P22	0.287	0.586	0.489	0.027941
ENSG00000080986.8	NDC80	0.758	1.637	0.463	0.028307
ENSG00000268598.1	VN1R80P	0.694	1.436	0.483	0.028491
ENSG00000122223.8	CD244	0.642	1.381	0.465	0.028492
ENSG00000169218.9	RSPO1	0.069	0.021	3.327	0.028715
ENSG00000159173.14	TNNI1	0.082	0.023	3.606	0.028744

ENSG00000205002.3	AARD	0.178	0.076	2.349	0.028754
ENSG00000102239.4	BRS3	0.036	0.012	3.005	0.028845
ENSG00000172938.3	MRGPRD	0.166	0.069	2.420	0.02889
ENSG00000233261.1	LINC00264	0.116	0.285	0.407	0.029358
ENSG00000152213.3	ARL11	0.662	1.324	0.500	0.029478
ENSG00000235129.1	FABP7P2	0.366	0.144	2.547	0.029613
ENSG00000144481.12	TRPM8	0.263	0.554	0.475	0.02981
ENSG00000138160.4	KIF11	0.705	1.469	0.480	0.029926
ENSG00000154975.9	CA10	7.075	3.355	2.109	0.030006
ENSG00000197616.7	MYH6	0.042	0.007	5.903	0.03013
ENSG00000232417.5	CT45A3	0.737	0.259	2.850	0.030538
ENSG00000006116.3	CACNG3	5.267	2.605	2.022	0.030579
ENSG00000231784.4	DBIL5P	0.984	0.481	2.045	0.030714
ENSG00000171551.7	ECEL1	0.264	0.112	2.350	0.030833
ENSG00000271956.1	DLX6-AS2	0.156	0.055	2.840	0.030847
ENSG00000174946.5	GPR171	2.984	1.466	2.036	0.031234
ENSG00000211956.2	IGHV4-34	0.406	3.321	0.122	0.0319
ENSG00000256316.1	HIST1H3F	4.580	13.161	0.348	0.031967
ENSG00000135426.10	TESPA1	9.804	4.885	2.007	0.031982
ENSG00000211666.2	IGLV2-14	2.394	17.935	0.133	0.032099
ENSG00000143632.10	ACTA1	1.716	0.525	3.268	0.032209
ENSG00000185482.3	STAC3	1.305	2.831	0.461	0.03234
ENSG00000178999.8	AURKB	0.541	1.346	0.402	0.03305
ENSG00000174576.4	NPAS4	20.761	5.020	4.136	0.033282
ENSG00000222004.3	C7orf71	0.109	0.229	0.474	0.033308
ENSG00000074966.6	TXK	0.865	1.896	0.457	0.033352
ENSG00000235076.2	GAPDHP52	0.129	0.274	0.472	0.033909
ENSG00000184408.5	KCND2	4.132	2.022	2.043	0.033992
ENSG00000179363.6	TMEM31	0.156	0.076	2.060	0.034254
ENSG00000134115.8	CNTN6	1.514	0.700	2.163	0.034266
ENSG00000237152.2	DLEU7-AS1	0.272	0.561	0.485	0.034298
ENSG00000223414.2	LINC00473	3.683	1.719	2.142	0.034442
ENSG00000101825.7	MXRA5	4.520	10.106	0.447	0.034526
ENSG00000153303.12	FRMD1	0.169	0.079	2.134	0.034726
ENSG00000138778.7	CENPE	0.649	1.351	0.480	0.034749
ENSG00000119283.11	TRIM67	0.636	0.261	2.438	0.034901
ENSG00000105549.6	THEG	0.100	0.042	2.373	0.035013
ENSG00000240183.2	RN7SL297P	0.776	1.724	0.450	0.03507
ENSG00000024526.12	DEPDC1	0.188	0.506	0.371	0.035105

ENSG00000079841.14	RIMS1	18.421	8.261	2.230	0.035436
ENSG00000171320.10	ESCO2	0.314	0.919	0.342	0.035437
ENSG00000134595.6	SOX3	0.066	0.026	2.575	0.036208
ENSG00000166863.7	TAC3	2.912	1.451	2.007	0.036323
ENSG00000227477.1	STK4-AS1	0.088	0.178	0.495	0.036348
ENSG00000183742.8	MACC1	0.632	1.329	0.475	0.036704
ENSG00000110148.5	CCKBR	2.651	1.319	2.009	0.036785
ENSG00000172724.7	CCL19	37.792	18.598	2.032	0.037114
ENSG00000134690.6	CDCA8	0.348	0.696	0.499	0.037148
ENSG00000101057.11	MYBL2	0.328	1.144	0.287	0.037604
ENSG00000003137.4	CYP26B1	11.011	5.314	2.072	0.037625
ENSG00000182611.3	HIST1H2AJ	2.379	8.581	0.277	0.037841
ENSG00000175879.7	HOXD8	0.131	0.382	0.342	0.037977
ENSG00000145386.5	CCNA2	0.605	1.394	0.434	0.038007
ENSG00000167613.11	LAIR1	21.365	43.614	0.490	0.038351
ENSG00000163331.6	DAPL1	2.548	1.117	2.281	0.038393
ENSG00000178462.7	TUBAL3	0.056	0.026	2.176	0.038525
ENSG00000204291.6	COL15A1	9.049	19.180	0.472	0.038643
ENSG00000101292.6	PROKR2	0.365	0.174	2.093	0.038752
ENSG00000158402.14	CDC25C	0.173	0.356	0.486	0.03892
ENSG00000110975.4	SYT10	0.378	0.181	2.094	0.039013
ENSG00000206014.5	OR7E161P	0.091	0.036	2.508	0.039249
ENSG00000179046.4	TRIML2	0.094	0.044	2.124	0.039313
ENSG00000027644.4	INSRR	1.075	0.528	2.037	0.039349
ENSG00000130035.2	GALNT8	2.436	1.134	2.149	0.039719
ENSG00000218698.1	ST13P16	0.165	0.079	2.105	0.040044
ENSG00000211663.2	IGLV3-19	1.086	6.359	0.171	0.040235
ENSG00000186185.9	KIF18B	0.271	0.647	0.418	0.040503
ENSG00000168078.5	PBK	0.188	0.768	0.245	0.040639
ENSG00000182156.5	ENPP7	0.046	0.109	0.428	0.040649
ENSG00000066279.12	ASPM	0.291	0.889	0.327	0.041036
ENSG00000230316.2	FEZF1-AS1	0.100	0.043	2.327	0.041518
ENSG00000166183.11	ASPG	0.251	0.121	2.082	0.041539
ENSG00000148677.6	ANKRD1	2.217	0.835	2.655	0.041548
ENSG00000147432.2	CHRNB3	0.413	0.171	2.409	0.041559
ENSG00000236062.1	GSTM5P1	0.222	0.099	2.254	0.041574
ENSG00000182572.2	HIST1H3I	4.752	14.066	0.338	0.042085
ENSG00000211821.2	TRDV2	0.191	0.522	0.365	0.042159
ENSG00000142945.8	KIF2C	0.632	1.278	0.494	0.042269

ENSG00000196183.4	RPS2P4	0.111	0.044	2.556	0.042341
ENSG00000197153.3	HIST1H3J	1.570	5.006	0.314	0.042527
ENSG00000188778.3	ADRB3	0.152	0.074	2.065	0.04265
ENSG00000121933.13	ADORA3	10.490	23.524	0.446	0.042746
ENSG00000211788.2	TRAV13-1	0.265	0.661	0.402	0.042902
ENSG00000175325.2	PROP1	0.091	0.035	2.587	0.043057
ENSG00000196747.3	HIST1H2AI	5.424	15.676	0.346	0.043415
ENSG00000137077.3	CCL21	5.297	2.603	2.035	0.043434
ENSG00000240048.1	DDX50P2	0.046	0.020	2.284	0.043601
ENSG00000164794.4	KCNV1	3.123	1.524	2.050	0.043622
ENSG00000213423.4	RBMX2P2	0.056	0.153	0.364	0.043692
ENSG00000089199.5	CHGB	23.824	11.731	2.031	0.043791
ENSG00000196132.7	MYT1	1.346	0.591	2.277	0.043805
ENSG00000118193.7	KIF14	0.173	0.451	0.384	0.043869
ENSG00000243137.3	PSG4	0.264	0.129	2.042	0.043903
ENSG00000163395.12	IGFN1	2.534	0.997	2.541	0.044013
ENSG00000148773.8	MKI67	0.722	2.334	0.310	0.044175
ENSG00000132821.7	VSTM2L	14.679	7.060	2.079	0.044221
ENSG00000134762.12	DSC3	0.301	0.134	2.252	0.044448
ENSG00000198558.2	HIST1H4L	4.528	10.743	0.421	0.044712
ENSG00000258548.1	LINC00645	0.111	0.052	2.120	0.044796
ENSG00000135625.6	EGR4	7.491	2.233	3.355	0.044845
ENSG00000159166.9	LAD1	0.096	0.221	0.436	0.044938
ENSG00000240541.2	TM4SF1-AS1	0.234	0.115	2.031	0.044952
ENSG00000118640.6	VAMP8	18.034	40.739	0.443	0.045152
ENSG00000258555.2	SPECC1L -ADORA2A	0.308	0.145	2.121	0.045191
ENSG00000215475.3	SIAH3	0.750	0.347	2.160	0.045421
ENSG00000169777.5	TAS2R1	0.085	0.041	2.091	0.045447
ENSG00000211940.2	IGHV3-9	0.432	3.591	0.120	0.045465
ENSG00000232144.1	PSAT1P2	0.064	0.160	0.397	0.045582
ENSG00000234611.1	OR2AT2P	0.082	0.038	2.170	0.045695
ENSG00000250305.4	KIAA1456	10.051	4.379	2.295	0.045773
ENSG00000198829.5	SUCNR1	0.568	2.760	0.206	0.046493
ENSG00000109193.6	SULT1E1	0.052	0.267	0.196	0.046551
ENSG00000010327.6	STAB1	38.073	83.408	0.456	0.046582
ENSG00000242076.1	IGKV1-33	1.408	8.014	0.176	0.04668
ENSG00000203747.5	FCGR3A	29.148	59.196	0.492	0.046691
ENSG00000174083.13	PIK3R6	0.767	1.644	0.467	0.046905

ENSG00000157456.3	CCNB2	0.747	1.738	0.430	0.047054
ENSG00000090889.10	KIF4A	0.348	0.749	0.465	0.047117
ENSG00000231211.2	RPL17P49	0.601	0.242	2.480	0.047247
ENSG00000004809.9	SLC22A16	0.147	0.379	0.389	0.047269
ENSG00000255833.1	TIFAB	0.092	0.264	0.349	0.047368
ENSG00000174600.9	CMKLR1	10.782	21.840	0.494	0.047391
ENSG00000007968.6	E2F2	0.201	0.429	0.469	0.04743
ENSG00000077009.9	NMRK2	0.163	0.066	2.480	0.047639
ENSG00000258477.1	PPIAP6	0.198	0.399	0.496	0.047861
ENSG00000237697.2	LINC00312	4.808	2.322	2.070	0.047967
ENSG00000239577.2	RN7SL388P	0.377	0.873	0.432	0.048326
ENSG00000111206.8	FOXM1	1.075	2.322	0.463	0.04834
ENSG00000122859.4	NEUROG3	0.063	0.031	2.050	0.048365
ENSG00000189430.8	NCR1	0.239	0.496	0.481	0.048619
ENSG00000130701.3	RBBP8NL	0.057	0.019	2.971	0.048691
ENSG00000198374.3	HIST1H2AL	3.302	9.059	0.365	0.048731
ENSG00000126787.8	DLGAP5	0.282	1.026	0.275	0.048794
ENSG00000100721.6	TCL1A	0.149	0.373	0.401	0.049107
ENSG00000134757.4	DSG3	0.040	0.009	4.308	0.04915
ENSG00000197459.2	HIST1H2BH	5.450	14.621	0.373	0.049397
ENSG00000197629.5	MPEG1	13.408	29.311	0.457	0.049451
ENSG00000215498.4	FAM230B	0.057	0.021	2.649	0.049883

FPKM Indicates fragments per kilobase of exon per million fragments mapped; LFR, low flow rate; HFR, high flow rate; FC, fold change.

Table S3. GO and KEGG analysis enriched by upregulated genes in low flow rate bAVMs.

GeneSet	Description	P value
GO:0042127	regulation of cell proliferation	7.37E-05
GO:0050727	regulation of inflammatory response	7.72E-05
GO:0007267	cell-cell signaling	8.05E-05
GO:0032103	positive regulation of response to external stimulus	1.41E-04
GO:0061888	regulation of astrocyte activation	1.49E-04
GO:0033993	response to lipid	1.59E-04
GO:0050729	positive regulation of inflammatory response	1.63E-04
GO:0032101	regulation of response to external stimulus	1.76E-04
GO:0002675	positive regulation of acute inflammatory response	1.93E-04
GO:0038031	non-canonical Wnt signaling pathway via JNK cascade	2.22E-04
GO:0008285	negative regulation of cell proliferation	2.41E-04
GO:0009914	hormone transport	2.51E-04
GO:0038030	non-canonical Wnt signaling pathway via MAPK cascade	3.11E-04
GO:2000381	negative regulation of mesoderm development	4.13E-04
GO:0002673	regulation of acute inflammatory response	4.55E-04
GO:1901700	response to oxygen-containing compound	7.80E-04
GO:0043030	regulation of macrophage activation	9.74E-04
GO:0032722	positive regulation of chemokine production	0.001032
GO:0008283	cell proliferation	0.00125
GO:0010469	regulation of signaling receptor activity	0.001306
GO:0046879	hormone secretion	0.001341
GO:0046677	response to antibiotic	0.001431
GO:0048143	astrocyte activation	0.001522
GO:1903978	regulation of microglial cell activation	0.001522
GO:0042074	cell migration involved in gastrulation	0.001522
GO:0007188	adenylate cyclase-modulating G protein-coupled receptor signaling pathway	0.001535
GO:0046887	positive regulation of hormone secretion	0.001611
GO:0042542	response to hydrogen peroxide	0.001705
GO:0006954	inflammatory response	0.001775
GO:0007189	adenylate cyclase-activating G protein-coupled receptor signaling pathway	0.001903
GO:2000380	regulation of mesoderm development	0.001962
GO:0043491	protein kinase B signaling	0.002099
GO:0010647	positive regulation of cell communication	0.002304
GO:1902533	positive regulation of intracellular signal transduction	0.002304
GO:0008284	positive regulation of cell proliferation	0.002369

GO:0023056	positive regulation of signaling	0.002384
GO:0023019	signal transduction involved in regulation of gene expression	0.00272
GO:0051384	response to glucocorticoid	0.002723
GO:0030072	peptide hormone secretion	0.002753
GO:0032642	regulation of chemokine production	0.002788
GO:0007187	G protein-coupled receptor signaling pathway, coupled to cyclic nucleotide second messenger	0.002899
GO:1900120	regulation of receptor binding	0.002999
GO:0043567	regulation of insulin-like growth factor receptor signaling pathway	0.002999
GO:0002526	acute inflammatory response	0.003067
GO:0045597	positive regulation of cell differentiation	0.003124
GO:0003018	vascular process in circulatory system	0.003139
GO:0009636	response to toxic substance	0.003216
GO:1903532	positive regulation of secretion by cell	0.003415
GO:0051897	positive regulation of protein kinase B signaling	0.003439
GO:0032602	chemokine production	0.003626
GO:0042116	macrophage activation	0.003626
GO:0014068	positive regulation of phosphatidylinositol 3-kinase signaling	0.003626
GO:0046883	regulation of hormone secretion	0.003779
GO:0010817	regulation of hormone levels	0.003867
GO:0002793	positive regulation of peptide secretion	0.003901
GO:0150077	regulation of neuroinflammatory response	0.003912
GO:0031960	response to corticosteroid	0.00401
GO:0051240	positive regulation of multicellular organismal process	0.004233
GO:0001934	positive regulation of protein phosphorylation	0.004496
GO:0007369	gastrulation	0.004835
GO:0042493	response to drug	0.004895
GO:0051047	positive regulation of secretion	0.004959
GO:0032958	inositol phosphate biosynthetic process	0.005305
GO:0048710	regulation of astrocyte differentiation	0.005305
GO:0019933	cAMP-mediated signaling	0.005339
GO:0044093	positive regulation of molecular function	0.005686
GO:0031347	regulation of defense response	0.005728
GO:0080134	regulation of response to stress	0.005846
GO:0090277	positive regulation of peptide hormone secretion	0.005898
GO:0007202	activation of phospholipase C activity	0.006074
GO:0042327	positive regulation of phosphorylation	0.006182

GO:0060251	regulation of glial cell proliferation	0.006477
GO:0001774	microglial cell activation	0.006477
GO:0002269	leukocyte activation involved in inflammatory response	0.006477
GO:0048333	mesodermal cell differentiation	0.006477
GO:0021782	glial cell development	0.006619
GO:0019932	second-messenger-mediated signaling	0.006743
GO:0009967	positive regulation of signal transduction	0.006881
GO:0043114	regulation of vascular permeability	0.006891
GO:0007218	neuropeptide signaling pathway	0.007192
GO:0014002	astrocyte development	0.007317
GO:0035567	non-canonical Wnt signaling pathway	0.00739
GO:0048009	insulin-like growth factor receptor signaling pathway	0.007755
GO:0009719	response to endogenous stimulus	0.007833
GO:0071396	cellular response to lipid	0.008143
GO:0032956	regulation of actin cytoskeleton organization	0.008165
GO:0060416	response to growth hormone	0.008205
GO:0051345	positive regulation of hydrolase activity	0.008231
GO:0090276	regulation of peptide hormone secretion	0.008392
GO:0030073	insulin secretion	0.008533
GO:0023061	signal release	0.008599
GO:0016055	Wnt signaling pathway	0.008599
GO:0051896	regulation of protein kinase B signaling	0.008676
GO:0019935	cyclic-nucleotide-mediated signaling	0.008821
GO:0198738	cell-cell signaling by Wnt	0.008865
GO:0014013	regulation of gliogenesis	0.009086
GO:0002791	regulation of peptide secretion	0.00923
GO:0061061	muscle structure development	0.009435
GO:0010562	positive regulation of phosphorus metabolic process	0.009603
GO:0045937	positive regulation of phosphate metabolic process	0.009603
GO:0061900	glial cell activation	0.009622
GO:0001704	formation of primary germ layer	0.009776
GO:0014066	regulation of phosphatidylinositol 3-kinase signaling	0.009776
GO:0051247	positive regulation of protein metabolic process	0.00981
GO:0000302	response to reactive oxygen species	0.009878
GO:0014014	negative regulation of gliogenesis	0.010622
GO:0007186	G protein-coupled receptor signaling pathway	0.010641
GO:0014009	glial cell proliferation	0.011139
GO:0032880	regulation of protein localization	0.011502
GO:0010863	positive regulation of phospholipase C activity	0.011667

GO:0042551	neuron maturation	0.011667
GO:0009725	response to hormone	0.011949
GO:0051094	positive regulation of developmental process	0.012115
GO:0042325	regulation of phosphorylation	0.012309
GO:0019220	regulation of phosphate metabolic process	0.012449
GO:0007498	mesoderm development	0.012564
GO:0051174	regulation of phosphorus metabolic process	0.012566
GO:0097305	response to alcohol	0.012595
GO:0002437	inflammatory response to antigenic stimulus	0.012755
GO:0032355	response to estradiol	0.013114
GO:1900274	regulation of phospholipase C activity	0.013315
GO:0009790	embryo development	0.01337
GO:0032970	regulation of actin filament-based process	0.013409
GO:0006952	defense response	0.013445
GO:0044703	multi-organism reproductive process	0.01387
GO:0034260	negative regulation of GTPase activity	0.013885
GO:2000026	regulation of multicellular organismal development	0.013948
GO:0050921	positive regulation of chemotaxis	0.014257
GO:0045944	positive regulation of transcription by RNA polymerase II	0.01449
GO:0051962	positive regulation of nervous system development	0.014613
GO:0045860	positive regulation of protein kinase activity	0.014742
GO:0001503	ossification	0.014773
GO:0009991	response to extracellular stimulus	0.015002
GO:0010720	positive regulation of cell development	0.015002
GO:0150076	neuroinflammatory response	0.015058
GO:0032270	positive regulation of cellular protein metabolic process	0.015156
GO:0007169	transmembrane receptor protein tyrosine kinase signaling pathway	0.015904
GO:0050714	positive regulation of protein secretion	0.016177
GO:0001706	endoderm formation	0.016271
GO:0031401	positive regulation of protein modification process	0.016332
GO:0014065	phosphatidylinositol 3-kinase signaling	0.016389
GO:0043085	positive regulation of catalytic activity	0.016987
GO:0051091	positive regulation of DNA-binding transcription factor activity	0.0175
GO:0048545	response to steroid hormone	0.017599
GO:0001932	regulation of protein phosphorylation	0.017665
GO:0035051	cardiocyte differentiation	0.017683
GO:0008277	regulation of G protein-coupled receptor signaling	0.01869

	pathway	
GO:0002865	negative regulation of acute inflammatory response to antigenic stimulus	0.019354
GO:0071651	positive regulation of chemokine (C-C motif) ligand 5 production	0.019354
GO:0090118	receptor-mediated endocytosis involved in cholesterol transport	0.019354
GO:0031547	brain-derived neurotrophic factor receptor signaling pathway	0.019354
GO:0080184	response to phenylpropanoid	0.019354
GO:0003307	regulation of Wnt signaling pathway involved in heart development	0.019354
GO:1904352	positive regulation of protein catabolic process in the vacuole	0.019354
GO:0030263	apoptotic chromosome condensation	0.019354
GO:0010641	positive regulation of platelet-derived growth factor receptor signaling pathway	0.019354
GO:0060664	epithelial cell proliferation involved in salivary gland morphogenesis	0.019354
GO:2000660	negative regulation of interleukin-1-mediated signaling pathway	0.019354
GO:1900223	positive regulation of amyloid-beta clearance	0.019354
GO:1900145	regulation of nodal signaling pathway involved in determination of left/right asymmetry	0.019354
GO:1900175	regulation of nodal signaling pathway involved in determination of lateral mesoderm left/right asymmetry	0.019354
GO:0038169	somatostatin receptor signaling pathway	0.019354
GO:0038170	somatostatin signaling pathway	0.019354
GO:0071557	histone H3-K27 demethylation	0.019354
GO:0043410	positive regulation of MAPK cascade	0.019444
GO:0042063	gliogenesis	0.019851
GO:0009306	protein secretion	0.020076
GO:0051960	regulation of nervous system development	0.020487
GO:0033674	positive regulation of kinase activity	0.02056
GO:0070555	response to interleukin-1	0.020799
GO:1903530	regulation of secretion by cell	0.020818
GO:0030029	actin filament-based process	0.020961
GO:1905114	cell surface receptor signaling pathway involved in cell-cell signaling	0.021383
GO:0010518	positive regulation of phospholipase activity	0.021524

GO:0046173	polyol biosynthetic process	0.021524
GO:1902531	regulation of intracellular signal transduction	0.022305
GO:1901701	cellular response to oxygen-containing compound	0.022926
GO:0071385	cellular response to glucocorticoid stimulus	0.022933
GO:0010986	positive regulation of lipoprotein particle clearance	0.02318
GO:0060696	regulation of phospholipid catabolic process	0.02318
GO:0043569	negative regulation of insulin-like growth factor receptor signaling pathway	0.02318
GO:0060770	negative regulation of epithelial cell proliferation involved in prostate gland development	0.02318
GO:0001957	intramembranous ossification	0.02318
GO:0036072	direct ossification	0.02318
GO:1904587	response to glycoprotein	0.02318
GO:0098914	membrane repolarization during atrial cardiac muscle cell action potential	0.02318
GO:2000553	positive regulation of T-helper 2 cell cytokine production	0.02318
GO:0003160	endocardium morphogenesis	0.02318
GO:0150079	negative regulation of neuroinflammatory response	0.02318
GO:0009996	negative regulation of cell fate specification	0.02318
GO:0048598	embryonic morphogenesis	0.023629
GO:0051093	negative regulation of developmental process	0.023916
GO:0045685	regulation of glial cell differentiation	0.025116
GO:0031349	positive regulation of defense response	0.025388
GO:0048015	phosphatidylinositol-mediated signaling	0.025394
GO:0043408	regulation of MAPK cascade	0.025551
GO:0002790	peptide secretion	0.02565
GO:0071384	cellular response to corticosteroid stimulus	0.025862
GO:0061371	determination of heart left/right asymmetry	0.025862
GO:0034097	response to cytokine	0.026275
GO:0014823	response to activity	0.026617
GO:0048017	inositol lipid-mediated signaling	0.026622
GO:0003348	cardiac endothelial cell differentiation	0.026992
GO:0060956	endocardial cell differentiation	0.026992
GO:1903997	positive regulation of non-membrane spanning protein tyrosine kinase activity	0.026992
GO:0015793	glycerol transport	0.026992
GO:0042661	regulation of mesodermal cell fate specification	0.026992
GO:1905770	regulation of mesodermal cell differentiation	0.026992
GO:1905902	regulation of mesoderm formation	0.026992
GO:0060372	regulation of atrial cardiac muscle cell membrane	0.026992

	repolarization	
GO:0086028	bundle of His cell to Purkinje myocyte signaling	0.026992
GO:0086043	bundle of His cell action potential	0.026992
GO:2000542	negative regulation of gastrulation	0.026992
GO:0071694	maintenance of protein location in extracellular region	0.026992
GO:0035766	cell chemotaxis to fibroblast growth factor	0.026992
GO:0035768	endothelial cell chemotaxis to fibroblast growth factor	0.026992
GO:1904847	regulation of cell chemotaxis to fibroblast growth factor	0.026992
GO:2000544	regulation of endothelial cell chemotaxis to fibroblast growth factor	0.026992
GO:0009249	protein lipoylation	0.026992
GO:0099004	calmodulin dependent kinase signaling pathway	0.026992
GO:2000659	regulation of interleukin-1-mediated signaling pathway	0.026992
GO:0002826	negative regulation of T-helper 1 type immune response	0.026992
GO:0038107	nodal signaling pathway involved in determination of left/right asymmetry	0.026992
GO:1900094	regulation of transcription from RNA polymerase II promoter involved in determination of left/right symmetry	0.026992
GO:1900164	nodal signaling pathway involved in determination of lateral mesoderm left/right asymmetry	0.026992
GO:0045162	clustering of voltage-gated sodium channels	0.026992
GO:0001826	inner cell mass cell differentiation	0.026992
GO:0051965	positive regulation of synapse assembly	0.027381
GO:0050708	regulation of protein secretion	0.027456
GO:0051050	positive regulation of transport	0.02789
GO:0001707	mesoderm formation	0.028153
GO:0045893	positive regulation of transcription, DNA-templated	0.02934
GO:0060193	positive regulation of lipase activity	0.029725
GO:0048332	mesoderm morphogenesis	0.029725
GO:0043647	inositol phosphate metabolic process	0.029725
GO:0045595	regulation of cell differentiation	0.029888
GO:0051046	regulation of secretion	0.030057
GO:0050769	positive regulation of neurogenesis	0.030126
GO:0050796	regulation of insulin secretion	0.030493
GO:0048708	astrocyte differentiation	0.030523
GO:0010517	regulation of phospholipase activity	0.030523
GO:0060350	endochondral bone morphogenesis	0.030523
GO:0007417	central nervous system development	0.030618
GO:0061476	response to anticoagulant	0.030789
GO:0070444	oligodendrocyte progenitor proliferation	0.030789

GO:0070445	regulation of oligodendrocyte progenitor proliferation	0.030789
GO:1903995	regulation of non-membrane spanning protein tyrosine kinase activity	0.030789
GO:0071692	protein localization to extracellular region	0.030789
GO:0001781	neutrophil apoptotic process	0.030789
GO:0034638	phosphatidylcholine catabolic process	0.030789
GO:1905906	regulation of amyloid fibril formation	0.030789
GO:2000288	positive regulation of myoblast proliferation	0.030789
GO:0070327	thyroid hormone transport	0.030789
GO:1900107	regulation of nodal signaling pathway	0.030789
GO:1905165	regulation of lysosomal protein catabolic process	0.030789
GO:0003140	determination of left/right asymmetry in lateral mesoderm	0.030789
GO:0001714	endodermal cell fate specification	0.030789
GO:0032024	positive regulation of insulin secretion	0.03133
GO:0043507	positive regulation of JUN kinase activity	0.032146
GO:0031328	positive regulation of cellular biosynthetic process	0.032269
GO:0007422	peripheral nervous system development	0.033802
GO:0007492	endoderm development	0.033802
GO:0048262	determination of dorsal/ventral asymmetry	0.034571
GO:0048263	determination of dorsal identity	0.034571
GO:0048617	embryonic foregut morphogenesis	0.034571
GO:0035907	dorsal aorta development	0.034571
GO:0042117	monocyte activation	0.034571
GO:0060124	positive regulation of growth hormone secretion	0.034571
GO:0071649	regulation of chemokine (C-C motif) ligand 5 production	0.034571
GO:0051901	positive regulation of mitochondrial depolarization	0.034571
GO:0086015	SA node cell action potential	0.034571
GO:0086018	SA node cell to atrial cardiac muscle cell signaling	0.034571
GO:1900122	positive regulation of receptor binding	0.034571
GO:0035376	sterol import	0.034571
GO:0070508	cholesterol import	0.034571
GO:0034382	chylomicron remnant clearance	0.034571
GO:0071830	triglyceride-rich lipoprotein particle clearance	0.034571
GO:1900221	regulation of amyloid-beta clearance	0.034571
GO:0048865	stem cell fate commitment	0.034571
GO:2000674	regulation of type B pancreatic cell apoptotic process	0.034571
GO:2000035	regulation of stem cell division	0.034571
GO:0035581	sequestering of extracellular ligand from receptor	0.034571
GO:0040011	locomotion	0.034827

GO:0051347	positive regulation of transferase activity	0.034886
GO:0050731	positive regulation of peptidyl-tyrosine phosphorylation	0.035124
GO:0032496	response to lipopolysaccharide	0.035164
GO:0048585	negative regulation of response to stimulus	0.035544
GO:0009891	positive regulation of biosynthetic process	0.03601
GO:0008015	blood circulation	0.036511
GO:1901654	response to ketone	0.037568
GO:0007167	enzyme linked receptor protein signaling pathway	0.037757
GO:0046470	phosphatidylcholine metabolic process	0.038084
GO:0032926	negative regulation of activin receptor signaling pathway	0.038339
GO:0007440	foregut morphogenesis	0.038339
GO:0071609	chemokine (C-C motif) ligand 5 production	0.038339
GO:0031340	positive regulation of vesicle fusion	0.038339
GO:0086070	SA node cell to atrial cardiac muscle cell communication	0.038339
GO:0060768	regulation of epithelial cell proliferation involved in prostate gland development	0.038339
GO:2000551	regulation of T-helper 2 cell cytokine production	0.038339
GO:0051481	negative regulation of cytosolic calcium ion concentration	0.038339
GO:0048672	positive regulation of collateral sprouting	0.038339
GO:0003306	Wnt signaling pathway involved in heart development	0.038339
GO:2000833	positive regulation of steroid hormone secretion	0.038339
GO:0099624	atrial cardiac muscle cell membrane repolarization	0.038339
GO:0097050	type B pancreatic cell apoptotic process	0.038339
GO:1904350	regulation of protein catabolic process in the vacuole	0.038339
GO:0070091	glucagon secretion	0.038339
GO:0030432	peristalsis	0.038339
GO:0007028	cytoplasm organization	0.038339
GO:0032966	negative regulation of collagen biosynthetic process	0.038339
GO:0006928	movement of cell or subcellular component	0.038402
GO:0032755	positive regulation of interleukin-6 production	0.038964
GO:0003013	circulatory system process	0.039106
GO:0002237	response to molecule of bacterial origin	0.039825
GO:0021766	hippocampus development	0.039852
GO:0019953	sexual reproduction	0.039962
GO:0050878	regulation of body fluid levels	0.039996
GO:0031667	response to nutrient levels	0.039996
GO:0010001	glial cell differentiation	0.041134
GO:1903508	positive regulation of nucleic acid-templated transcription	0.041338
GO:1902680	positive regulation of RNA biosynthetic process	0.041499

GO:0030155	regulation of cell adhesion	0.041767
GO:0002862	negative regulation of inflammatory response to antigenic stimulus	0.042092
GO:1904181	positive regulation of membrane depolarization	0.042092
GO:0040015	negative regulation of multicellular organism growth	0.042092
GO:0016322	neuron remodeling	0.042092
GO:0015791	polyol transport	0.042092
GO:0060767	epithelial cell proliferation involved in prostate gland development	0.042092
GO:0045073	regulation of chemokine biosynthetic process	0.042092
GO:0060992	response to fungicide	0.042092
GO:0009629	response to gravity	0.042092
GO:0032494	response to peptidoglycan	0.042092
GO:0010713	negative regulation of collagen metabolic process	0.042092
GO:0018065	protein-cofactor linkage	0.042092
GO:0048712	negative regulation of astrocyte differentiation	0.042092
GO:1905146	lysosomal protein catabolic process	0.042092
GO:0010454	negative regulation of cell fate commitment	0.042092
GO:0002690	positive regulation of leukocyte chemotaxis	0.042561
GO:1903725	regulation of phospholipid metabolic process	0.042561
GO:0051130	positive regulation of cellular component organization	0.043009
GO:0070301	cellular response to hydrogen peroxide	0.04348
GO:0043549	regulation of kinase activity	0.043614
GO:0022414	reproductive process	0.04428
GO:0043506	regulation of JUN kinase activity	0.044405
GO:0000003	reproduction	0.044823
GO:0001649	osteoblast differentiation	0.044866
GO:0051493	regulation of cytoskeleton organization	0.045272
GO:0072359	circulatory system development	0.045303
GO:0038166	angiotensin-activated signaling pathway	0.045831
GO:0060911	cardiac cell fate commitment	0.045831
GO:0003157	endocardium development	0.045831
GO:0002523	leukocyte migration involved in inflammatory response	0.045831
GO:0038003	opioid receptor signaling pathway	0.045831
GO:0002674	negative regulation of acute inflammatory response	0.045831
GO:0030950	establishment or maintenance of actin cytoskeleton polarity	0.045831
GO:0060081	membrane hyperpolarization	0.045831
GO:0042033	chemokine biosynthetic process	0.045831

GO:0050755	chemokine metabolic process	0.045831
GO:1900121	negative regulation of receptor binding	0.045831
GO:0007288	sperm axoneme assembly	0.045831
GO:0038180	nerve growth factor signaling pathway	0.045831
GO:0060442	branching involved in prostate gland morphogenesis	0.045831
GO:0043031	negative regulation of macrophage activation	0.045831
GO:0045779	negative regulation of bone resorption	0.045831
GO:0010867	positive regulation of triglyceride biosynthetic process	0.045831
GO:0021903	rostrocaudal neural tube patterning	0.045831
GO:0051024	positive regulation of immunoglobulin secretion	0.045831
GO:0072540	T-helper 17 cell lineage commitment	0.045831
GO:0045161	neuronal ion channel clustering	0.045831
GO:0050920	regulation of chemotaxis	0.045962
GO:0007276	gamete generation	0.047458
GO:0060348	bone development	0.047631
GO:0045666	positive regulation of neuron differentiation	0.047657
GO:0010557	positive regulation of macromolecule biosynthetic process	0.048101
GO:0009952	anterior/posterior pattern specification	0.04933
GO:0002864	regulation of acute inflammatory response to antigenic stimulus	0.049556
GO:0060123	regulation of growth hormone secretion	0.049556
GO:0090197	positive regulation of chemokine secretion	0.049556
GO:0030299	intestinal cholesterol absorption	0.049556
GO:0034384	high-density lipoprotein particle clearance	0.049556
GO:0042159	lipoprotein catabolic process	0.049556
GO:0043568	positive regulation of insulin-like growth factor receptor signaling pathway	0.049556
GO:0042659	regulation of cell fate specification	0.049556
GO:0035745	T-helper 2 cell cytokine production	0.049556
GO:2000291	regulation of myoblast proliferation	0.049556
GO:0090179	planar cell polarity pathway involved in neural tube closure	0.049556
GO:0061029	eyelid development in camera-type eye	0.049556
GO:0032754	positive regulation of interleukin-5 production	0.049556
GO:0051336	regulation of hydrolase activity	0.050484
GO:0014706	striated muscle tissue development	0.050587
GO:0008406	gonad development	0.051059
GO:0032092	positive regulation of protein binding	0.051086
GO:0032870	cellular response to hormone stimulus	0.051511
	positive regulation of nucleobase-containing compound	

GO:0045935	metabolic process	0.051733
GO:0060191	regulation of lipase activity	0.052068
GO:0043393	regulation of protein binding	0.052228
GO:0090087	regulation of peptide transport	0.053009
GO:0043266	regulation of potassium ion transport	0.053058
GO:0001821	histamine secretion	0.053266
GO:0060732	positive regulation of inositol phosphate biosynthetic process	0.053266
GO:0150078	positive regulation of neuroinflammatory response	0.053266
GO:0019372	lipoxygenase pathway	0.053266
GO:0090196	regulation of chemokine secretion	0.053266
GO:0098856	intestinal lipid absorption	0.053266
GO:0010273	detoxification of copper ion	0.053266
GO:1990169	stress response to copper ion	0.053266
GO:0007501	mesodermal cell fate specification	0.053266
GO:0086069	bundle of His cell to Purkinje myocyte communication	0.053266
GO:0046851	negative regulation of bone remodeling	0.053266
GO:0071850	mitotic cell cycle arrest	0.053266
GO:0090178	regulation of establishment of planar polarity involved in neural tube closure	0.053266
GO:0001675	acrosome assembly	0.053266
GO:0007283	spermatogenesis	0.053403
GO:0044706	multi-multicellular organism process	0.05341
GO:0044089	positive regulation of cellular component biogenesis	0.05376
GO:0120162	positive regulation of cold-induced thermogenesis	0.054053
GO:0010876	lipid localization	0.054056
GO:0006468	protein phosphorylation	0.054075
GO:0048699	generation of neurons	0.054159
GO:0045137	development of primary sexual characteristics	0.054604
GO:0048646	anatomical structure formation involved in morphogenesis	0.054771
GO:0006650	glycerophospholipid metabolic process	0.05539
GO:0051254	positive regulation of RNA metabolic process	0.056649
GO:0060537	muscle tissue development	0.056741
GO:0051608	histamine transport	0.056962
GO:0060253	negative regulation of glial cell proliferation	0.056962
GO:0044241	lipid digestion	0.056962
GO:1990000	amyloid fibril formation	0.056962
GO:0030949	positive regulation of vascular endothelial growth factor receptor signaling pathway	0.056962

GO:0061687	detoxification of inorganic compound	0.056962
GO:0048368	lateral mesoderm development	0.056962
GO:0002830	positive regulation of type 2 immune response	0.056962
GO:0007039	protein catabolic process in the vacuole	0.056962
GO:0001711	endodermal cell fate commitment	0.056962
GO:0090177	establishment of planar polarity involved in neural tube closure	0.056962
GO:2001028	positive regulation of endothelial cell chemotaxis	0.056962
GO:0050673	epithelial cell proliferation	0.057195
GO:0010035	response to inorganic substance	0.057772
GO:0007507	heart development	0.057772
GO:0030900	forebrain development	0.058571
GO:0060284	regulation of cell development	0.058941
GO:0000165	MAPK cascade	0.059226
GO:0048232	male gamete generation	0.060031
GO:0006813	potassium ion transport	0.060139
GO:0030252	growth hormone secretion	0.060644
GO:0010919	regulation of inositol phosphate biosynthetic process	0.060644
GO:0090195	chemokine secretion	0.060644
GO:0001780	neutrophil homeostasis	0.060644
GO:0030952	establishment or maintenance of cytoskeleton polarity	0.060644
GO:0048791	calcium ion-regulated exocytosis of neurotransmitter	0.060644
GO:0097501	stress response to metal ion	0.060644
GO:0060252	positive regulation of glial cell proliferation	0.060644
GO:0002295	T-helper cell lineage commitment	0.060644
GO:0043252	sodium-independent organic anion transport	0.060644
GO:0045446	endothelial cell differentiation	0.061207
GO:0033138	positive regulation of peptidyl-serine phosphorylation	0.061207
GO:0014070	response to organic cyclic compound	0.061834
GO:0051963	regulation of synapse assembly	0.062255
GO:0023014	signal transduction by protein phosphorylation	0.062423
GO:0061337	cardiac conduction	0.063308
GO:0018108	peptidyl-tyrosine phosphorylation	0.063765
GO:0010628	positive regulation of gene expression	0.063968
GO:0038092	nodal signaling pathway	0.064311
GO:0060644	mammary gland epithelial cell differentiation	0.064311
GO:0007567	parturition	0.064311
GO:0010866	regulation of triglyceride biosynthetic process	0.064311
GO:0070102	interleukin-6-mediated signaling pathway	0.064311

GO:0060850	regulation of transcription involved in cell fate commitment	0.064311
GO:0051450	myoblast proliferation	0.064311
GO:0042249	establishment of planar polarity of embryonic epithelium	0.064311
GO:0043373	CD4-positive, alpha-beta T cell lineage commitment	0.064311
GO:0018212	peptidyl-tyrosine modification	0.065223
GO:0009755	hormone-mediated signaling pathway	0.065272
GO:0021761	limbic system development	0.066505
GO:0007050	cell cycle arrest	0.067248
GO:0002688	regulation of leukocyte chemotaxis	0.067582
GO:0030182	neuron differentiation	0.06768
GO:0090208	positive regulation of triglyceride metabolic process	0.067965
GO:0071404	cellular response to low-density lipoprotein particle stimulus	0.067965
GO:2000251	positive regulation of actin cytoskeleton reorganization	0.067965
GO:0060749	mammary gland alveolus development	0.067965
GO:0061377	mammary gland lobule development	0.067965
GO:0002726	positive regulation of T cell cytokine production	0.067965
GO:0010832	negative regulation of myotube differentiation	0.067965
GO:0001710	mesodermal cell fate commitment	0.067965
GO:0007250	activation of NF-kappaB-inducing kinase activity	0.067965
GO:0071435	potassium ion export	0.067965
GO:0097623	potassium ion export across plasma membrane	0.067965
GO:1905276	regulation of epithelial tube formation	0.067965
GO:0036148	phosphatidylglycerol acyl-chain remodeling	0.067965
GO:0048878	chemical homeostasis	0.068515
GO:0048870	cell motility	0.068534
GO:0051674	localization of cell	0.068534
GO:0060349	bone morphogenesis	0.068665
GO:0007613	memory	0.069754
GO:0055007	cardiac muscle cell differentiation	0.069754
GO:0050730	regulation of peptidyl-tyrosine phosphorylation	0.069924
GO:0007611	learning or memory	0.069924
GO:0043547	positive regulation of GTPase activity	0.070718
GO:0046854	phosphatidylinositol phosphorylation	0.070849
KEGG: hsa05144	malaria - Homo sapiens (human)	0.000942
KEGG: hsa04310	Wnt signaling pathway - Homo sapiens (human)	0.002361
KEGG: hsa05143	African trypanosomiasis - Homo sapiens (human)	0.008511
KEGG: hsa04080	neuroactive ligand-receptor interaction - Homo sapiens	0.023739

	(human)	
KEGG: hsa04630	Jak-STAT signaling pathway - Homo sapiens (human)	0.024644

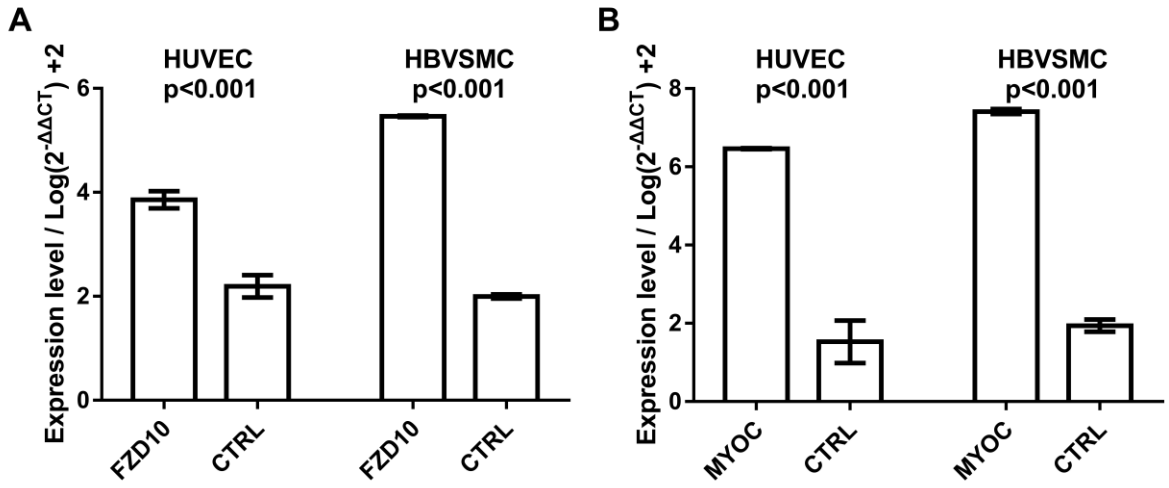

Figure S1. Expression level of FZD10 (A) and MYOC (B) in HUVECs and HBVSMCs after transfection.